Clinical and Biomedical Applications of Lensless Holographic Microscopy

Colin J. Potter Zhen Xiong Euan McLeod

C. J. Potter is with the James C. Wyant College of Optical Sciences and the College of Medicine - Tucson at the University of Arizona, Tucson, AZ 85721 USA (e-mail: colinjpotter@arizona.edu).
E. McLeod is with the James C. Wyant College of Optical Sciences and the BIO5 Institute at the University of Arizona, Tucson, AZ 85721 USA.(e-mail: euanmc@optics.arizona.edu).
Z. Xiong was with the James C. Wyant College of Optical Sciences at the University of Arizona, Tucson, AZ 85721 USA. He is now an Independent Researcher, San Jose, CA 95128 USA (e-mail: zxiong@optics.arizona.

Keywords: *lensless holographic microscopy, pathology, cytometry, infectious disease, biosensing, live-cell imaging, cell viability, drug discovery*

Many clinical procedures and biomedical research workflows rely on microscopy, including diagnosis of cancer, genetic disorders, autoimmune diseases, infections, and quantification of cell culture. Despite its widespread use, traditional image acquisition and review by trained microscopists is often lengthy and expensive, limited to large hospitals or laboratories, precluding use in point-of-care settings. In contrast, lensless or lensfree holographic microscopy (LHM) is inexpensive and widely deployable because it can achieve performance comparable to expensive and bulky objective-based benchtop microscopes while relying on components that cost only a few hundred dollars or less. Lab-on-a-chip integration is practical and enables LHM to be combined with single-cell isolation, sample mixing, and in-incubator imaging. Additionally, many manual tasks in conventional microscopy are instead computational in LHM, including image focusing, stitching, and classification. Furthermore, LHM offers a field of view hundreds of times greater than that of conventional microscopy without sacrificing resolution. Here, we summarize the basic LHM principles as well as recent advances in artificial intelligence integration and enhanced resolution. We discuss in detail how LHM has been applied to the above clinical and biomedical applications. Finally, we identify emerging clinical applications, high-impact areas for future research, and some current challenges facing widespread adoption.

1 Introduction

Many clinical diagnostic procedures and biomedical research workflows rely on microscopic images of specimens. For instance, hematology and cytometry rely on images of individual cells and can be used to diagnose infections and diseases including malaria and cancer, as well as genetic disorders like hereditary anemias [1, 2]. Cancer researchers and pharmacological scientists rely on cell culture imaging to determine cell growth and viability [3]. Pathologists use stained and sectioned tissues to diagnose a variety of cancers, genetic disorders, and autoimmune diseases [4]. The use of microscopy is truly ubiquitous in clinical medicine and biomedical research and underpins our current understanding of the human body and medical treatments. Despite its widespread use, traditional image acquisition and review by trained microscopists is often lengthy and expensive, and limited to large hospitals or laboratories, precluding use in point-of-care (POC) or low-resource settings [5].
On the other hand, lensless or lensfree holographic microscopy (LHM)is an inexpensive and widely deployable technology because it can achieve performance comparable to expensive and bulky objective-based benchtop microscopes while relying on components that cost only a few hundred dollars or less [6]. LHM is a variant of digital holographic microscopy (DHM), which in turn is a type of quantitative phase imaging technology. DHM generally refers to imaging which utilizes platforms based on a Michelson or Mach-Zehnder interferometer configuration, where the sample is placed in one of the arms of the interferometer [7]. Lensless holographic imaging techniques eliminate the need for two light paths and beam splitters, producing holograms in an in-line configurations. Throughout the remainder of this review, LHM will be used to refer to techniques which use a light source that meets coherence requirements for hologram production (i.e. non-fluorescent imaging), similar to DHM. In the literature, other abbreviations for LHM have been used, including lensfree holographic microscopy (LFHM), lensless digital holographic microscopy (LDHM), lensless digital holography (LDH), and lensless in-line holographic microscopy (LIHM), all of which refer to the same technology. Due to the size and simplicity of the hardware, lab-on-a-chip integration is practical and enables LHM to be combined with single-cell isolation, sample mixing, and in-incubator imaging. Additionally, many tasks that are performed manually in conventional

microscopy are instead computational in LHM, including image focusing, image stitching, and feature identification and classification. Furthermore, LHM offers a field of view (FOV) hundreds of times greater than that of conventional microscopy without sacrificing resolution, a combination quantified as *space-bandwidth product*. For images, the space-bandwidth product is defined as the total image area divided by the square of the system resolution [8].

To date, several reviews of LHM techniques have been written. Other reviews on LHM have provided excellent overviews of technological advances in LHM, including basic LHM theory and reconstruction methodologies [6, 9, 10], novel resolution enhancement techniques [11, 12], and more advanced image processing and backpropagation algorithms [13, 14], but these reviews have missed some key recent developments. Primarily, no review published to date has made its focus to enumerate biomedical applications of LHM in adequate depth so as to fully convey the current state of LHM prevalence and impact on any given biomedical application. Reviews that have addressed biomedically relevant applications have done so sparingly and often at the end of a technical section, where applications are given as examples rather than as the driving factor behind particular technological advances best suited for the particular application. Furthermore, advances in LHM directed at biomedical applications that have occurred in the last five years are largely absent. Due to the rapidly evolving nature of the field, many high-impact LHM advances have indeed occurred in the last five years and often their development has been driven by the need to address a specific imaging problem presented by a clinical and biomedical application, including pathology, cellular cytometry, infectious disease, biosensing, live cell and cell culture analysis, pharmacological testing, and basic biological science.

In this review, we give a brief summary of basic principles shared across many LHM systems as well as some recent technological advances such as artificial intelligence integration and enhanced resolution techniques, and discuss in detail the ways in which these systems have been applied to the areas mentioned above. In each section, we discuss LHM systems that have been developed for use in a specific clinical medicine or biomedical research application, and we provide a commentary on the aspects of LHM that make it advantageous or disadvantageous for each application as well as design principles that are necessary or are shared by most LHM systems for success in each application. In providing this additional information, we hope to aid in the identification of effective strategies for targeted technological advancement of LHM and LHM translation in these fields. Finally, we identify emerging areas or applications of LHM in clinical diagnostic medicine and biomedical research, interesting advances in LHM technology that have not yet seen use in clinical or biomedical applications to date or that remain not fully explored, and the current challenges in the widespread adoption of LHM in clinical and biomedical fields.

2 Compelling and versatile aspects of lensless holographic microscopy

2.1 Typical LHM system design

Holography was coined to reflect that Gabor's work [15] captured both the amplitude and phase field information. The design Gabor used is often called in-line holography since both the reference wave (light passing through the transparent sample unperturbed) and the object wave (light scattered by objects that are being imaged) have the same optical axis.

A typical LHM system is illustrated in Figure 1. Key components includes a light source, which can be a laser diode (LD) [16], a light-emitting diode (LED) [17], or an array of LDs or LEDs [18]; a charge-coupled device (CCD) or complementary metal–oxide–semiconductor (CMOS) image sensor to capture holographic images digitally; spectral filters and/or pinholes/conical optical fiber ends to meet optical coherence requirements specific to each design; and holders or microfluidic chips for sample delivery [19–22].

The distance between the sample plane at z_s and the light source is denoted as z_1, which typically ranges from 5–30 cm. Therefore light at z_s can be approximated as plane waves, since the light source is approximately a point source. The separation between the image sensor plane z_i and z_s is denoted as $z_2 = |z_s - z_i|$, typically on the order of 10 μm to 1 mm. Separation distances at the lower end of this range

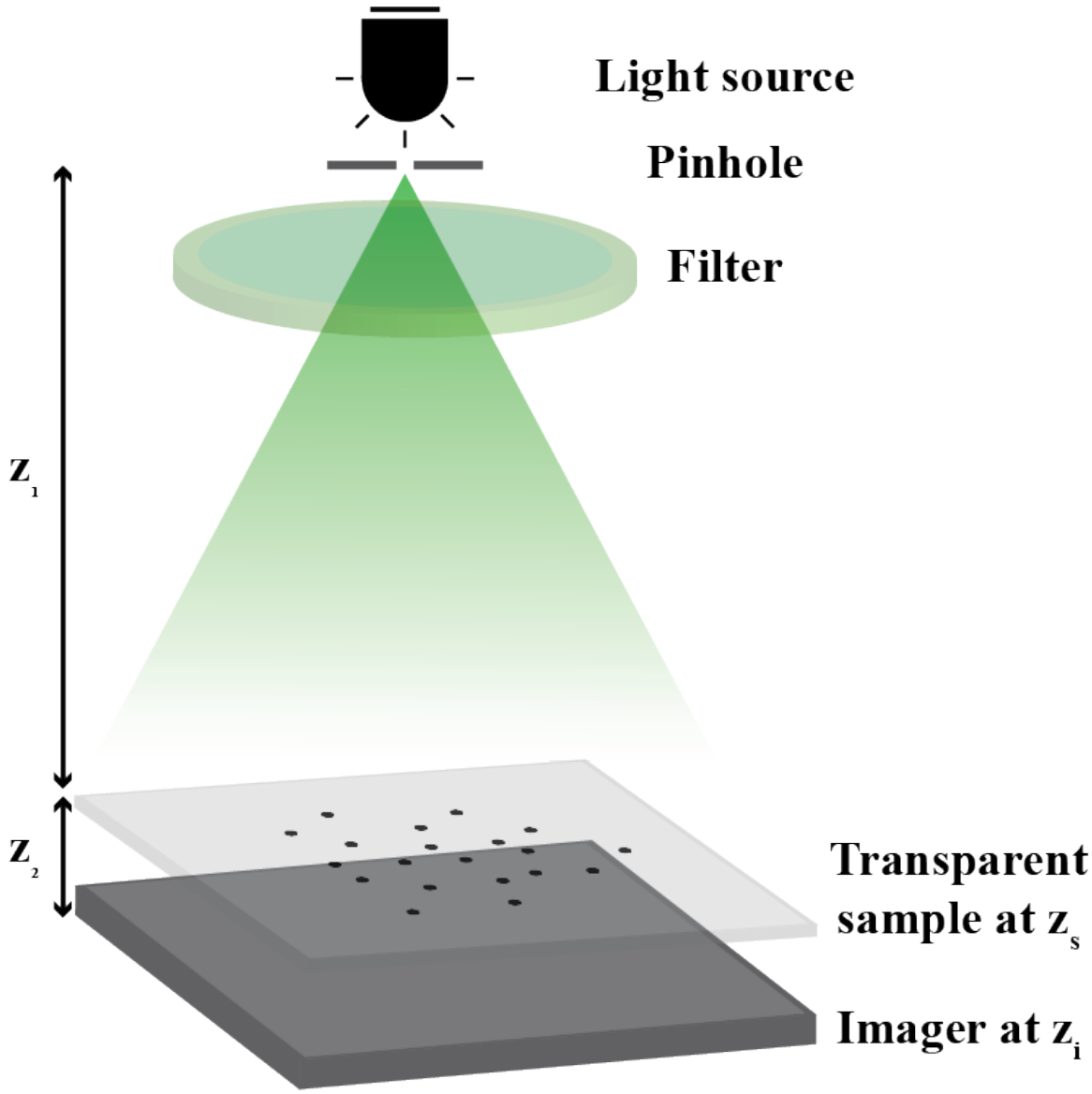

Figure 1: Basic in-line LHM schematic based on Gabor's initial in-line design with a light source, a sample (depicted here as red blood cells in a microfluidic channel, but this varies depending on the application), and an image sensor, a configuration shared across nearly all LHM devices.

may require professional removal of the protective cover glass found on many commercial image sensors. Several companies exist that can perform this service for a fee. Since $z_2 \ll z_1$, the FOV in a LHM system is equal to the active area of the image sensor, rather than limited by a lens field number. Commercially available modern CCD or CMOS image sensors have active areas ranging from a few square millimeters to > 100 mm^2.

Unlike in lens-based microscopy, where FOV is sacrificed to improve optical resolution, in LHM, resolution is mainly limited by image sensor pixel size and the optical coherence. In order to record a hologram digitally at the image sensor with strong fringe contrast, a LHM system must meet the coherence requirements, which are stated in Section 3.1 from [6]. Bandpass filters and pinholes are commonly utilized to improve temporal and spatial coherence respectively. In LHM systems with pixel size limited optical resolution, pixel super-resolution techniques [18] can be used to computationally meld multiple partially redundant sample images with subpixel shifts, achieving optical resolution finer than the image sensor pixel size. In lens-based microscopes, numerical aperture (NA) is commonly used to characterize optical resolution:

$$R \approx \frac{\lambda}{2\ \mathrm{NA}} = \frac{\lambda}{2n \sin\theta_{max}}, \tag{1}$$

where λ is wavelength, n represents refractive index, and, in the case of LHM, θ_{max} denotes the greatest angle where the reference and object waves meets temporal and spatial coherence requirements to exhibit interference effects at the image sensor plane z_i [6].

2.2 LHM reconstruction

As illustrated in Figure 1, a hologram $I(x, y, z_i)$ is recorded digitally at the image sensor since sensors can only record intensity information. Our goal is to computationally reconstruct the object wave $E_O(x, y, z_s)$ at the sample plane with both amplitude and phase information.
The recorded intensity image can be expressed as:

$$\begin{aligned} I(x,y,z_i) &= |E(x,y,z_i)|^2 \\ &= |E_R(x,y,z_i) + E_O(x,y,z_i)|^2 \\ &= |E_R(x,y,z_i)|^2 + E_R^*(x,y,z_i)E_O(x,y,z_i) \\ &+ E_R(x,y,z_i)E_O^*(x,y,z_i) + |E_O(x,y,z_i)|^2 \\ &= B_R^2 + B_R e^{-ikz_2}\mathcal{P}_{z_2}\big\{E_O(x,y,z_s)\big\} \\ &+ B_R e^{ikz_2}\big[\mathcal{P}_{z_2}\big\{E_O(x,y,z_s)\big\}\big]^* \\ &+ |\mathcal{P}_{z_2}\big\{E_O(x,y,z_s)\big\}|^2 \end{aligned} \tag{2}$$

where * is the complex conjugate operator, $k = \frac{2\pi n}{\lambda}$ is the wavenumber, B_R is a constant, the reference wave $E_R(x, y, z_i) = B_R e^{ikz_2}$ is a plane wave, and $\mathcal{P}_z$ is an operator denoting the forward propagation of light over a distance z, where $E(x, y, z) \equiv \mathcal{P}_z\big\{E(x, y, 0)\big\}$ can be calculated using the angular spectrum method [23] as:

$$E(x,y,z) = \mathcal{F}^{-1}\big\{\mathcal{F}\big\{E(x,y,0)\big\}H(\xi,\eta,z)\big\}, \tag{3}$$

with the transfer function in terms of spatial frequencies ξ and η defined as,

$$H(\xi,\eta,z) = \begin{cases} 0, & \text{for } \xi^2+\eta^2 \geq \frac{n^2}{\lambda^2} \\ e^{2\pi i z\sqrt{\frac{n^2}{\lambda^2}-\xi^2-\eta^2}}, & \text{otherwise.} \end{cases} \tag{4}$$

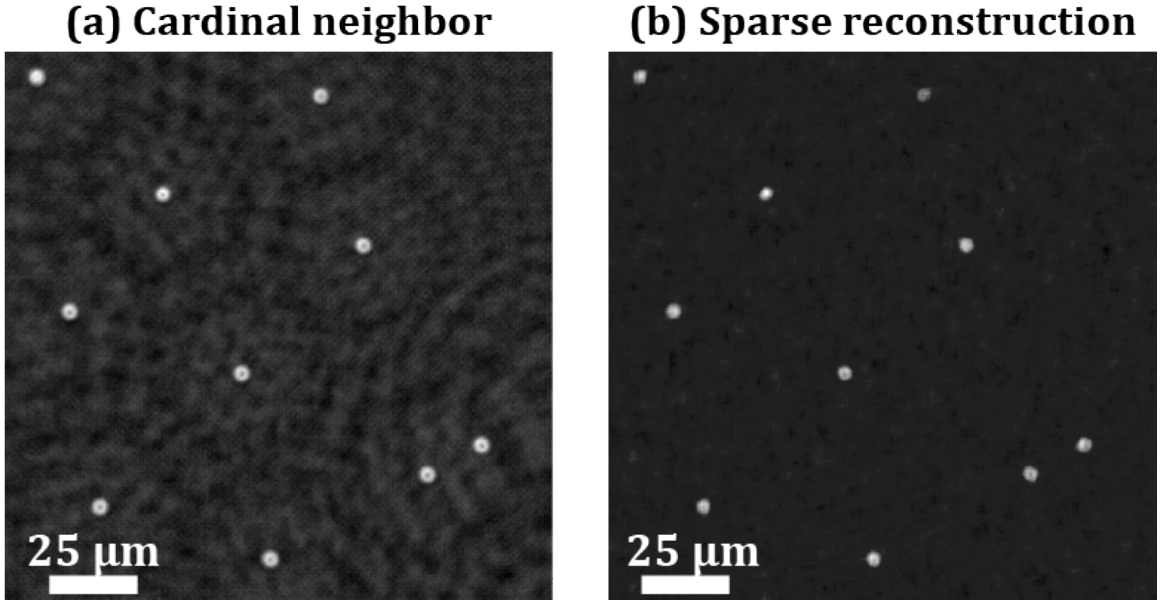

Figure 2: (a) PSR holographic reconstruction with cardinal neighbor regularization. The ring shape features around 5-µm microspheres are from the twin-image term. (b) PSR holographic reconstruction with sparse reconstruction regularization, where twin-image term is suppressed. Figure reproduced with permission from [18].

When the object wave is weak compared to the reference wave, which is generally valid except for dense or thick samples, $|\mathcal{P}_{z_2}\{E_O(x,y,z_s)\}|^2$ in Equation 2 can be neglected. To reconstruct an object image from the captured hologram, one can then back-propagate the recorded intensity image $I(x,y,z_i)$ over a distance of z_2 to the sample plane:

$$\begin{aligned}\mathcal{P}_{-z_2}\{I(x,y,z_i)\} &= B_R^2 e^{-ikz_2} \\ &+ B_R e^{-ikz_2} E_O(x,y,z_s) \\ &+ B_R e^{ikz_2} \mathcal{P}_{-z_2}\{[\mathcal{P}_{z_2}\{E_O(x,y,z_s)\}]^*\} \\ &\equiv E_{rec}(x,y,z_s).\end{aligned} \tag{5}$$

Since $\mathcal{P}_{-z}\{\mathcal{P}_z\{E\}\} = E$, therefore Equation 5 can be simplified as:

$$\begin{aligned}E_{rec}(x,y,z_s) &= B_R^2 e^{-ikz_2} + B_R e^{-ikz_2} E_O(x,y,z_s) \\ &+ B_R e^{ikz_2} \mathcal{P}_{-2z_2}\{E_O^*(x,y,z_s)\}.\end{aligned} \tag{6}$$

By back-propagating the recorded hologram, we are able to obtain the reconstructed field $E_{rec}(x,y,z_s)$ that contains our goal $E_O(x,y,z_s)$ along with a twin-image term. The twin-image term in Equation 6 can be thought of as the diffraction pattern from a "twin object" located also at a distance z_2 away from the image sensor, but on the opposite side of the sample. Various approaches towards eliminating artifacts from twin-image term are discussed in Section 2.4.

Equation 6 provides a way to compute $E_O(x,y,z_s)$ from a recorded hologram $I(x,y,z_i)$. In practice, fast Fourier transforms (FFTs) and inverse FFTs are used to efficiently implement Equation 3. Typically, reconstructions can be completed in ∼1 s with a typical consumer laptop [6]. In addition, graphics processing units (GPUs) can be used to significantly reduce computation time since FFTs can be implemented more efficiently on GPUs [24]. Over the years, the cost of computation has continued to decline rapidly [25], which benefits LHM both in performance and accessibility.

2.3 Pixel super-resolution

Pixel super-resolution (PSR) techniques have been frequently deployed to improve optical resolution beyond image sensor pixel size and to also improve the signal-to-noise ratio (SNR) of reconstructed images [18, 26, 27]. Note that because PSR techniques are performed on raw holographic images, the final reconstructed image will show improvements in both resolution and SNR. Multiple frames of the same scene with slight shifts between the frames are captured, providing a denser sampling of the electric field than image sensor pixel size.

In PSR, an LED array can be used as the light source, where each LED is turned on and off sequentially, illuminating the sample from slightly different angles. Multiple images of the same scene are captured, providing partially redundant information about the scene. Though PSR assumes a static scene, it was successfully used to image microspheres undergoing Brownian motion in solution [19].

Computationally, the process of synthesizing a high-resolution (HR) hologram from multiple low-resolution (LR) partially redundant holograms is an optimization problem. Denoting the HR hologram estimate as $\hat{I}$, then:

$$\hat{I} = \underset{I}{\arg\min} C(I), \tag{7}$$

where $C(I)$ is the cost function:

$$C(I) = e\{\mathrm{HR}, \mathrm{LR}\} + \kappa C_{reg}. \tag{8}$$

$e\{\mathrm{HR}, \mathrm{LR}\}$ denotes the error term between the HR hologram estimate and measured LR holograms. Since this optimization is an ill-posed problem, typically a regularization term C_{reg} is added to stabilize the PSR algorithm, with κ being the regularization weight. Various regularization methods are compared and a guide on choosing proper regularization methods is provided in [18].

Cardinal neighbor regularization and sparse reconstruction regularization methods are pertinent to most applications, as most samples are naturally smooth and/or sparse. Cardinal neighbor regularization penalizes nearest neighbor fluctuations in the HR hologram, while sparse reconstruction regularization promotes sparsity in the sample plane. PSR holographic reconstruction of 5-μm microspheres using cardinal neighbor and sparse reconstruction regularization methods are shown in Figure 2(a) and (b) respectively. The best demonstrated resolution in LHM systems used a synthetic aperture reconstruction approach to achieve a smallest resolvable feature size of approximately $\lambda/2.8$, or 250 nm, equivalent to the resolution of a 1.4 NA objective lens [28]. Future improvements to resolution may be possible by more accurately considering the light-matter interaction at the nanoscale [29]. Additionally, other PSR algorithms include those that operate in the frequency domain [30], and a sparsity-based fast-converging method termed accelerated Wirtinger flow for PSR phase retrieval [31].

2.4 Approaching the twin-image term and noise

Equation 6 states that the reconstructed field contains both the object term and the twin-image term. In off-axis holographic microscopy [32], the twin-image is spatially separated from the diffraction from the object and can be digitally removed with relative simplicity; however, for an in-line setup such as that shown in Figure 1, the twin image overlaps with the object image that one wishes to recover, making twin-image elimination more challenging.

In these in-line geometries, the twin-image term can be numerically suppressed using iterative algorithms [17]. If the hologram is naively reconstructed to the sample plane at $z = z_s = z_i - z_2$, as shown in Figure 2, then the twin image is apparent in the ring-shaped features around the 5-μm microspheres. If instead, the hologram was reconstructed to the $z = z_i + z_2$ plane, then the twin-image term would become in focus while the object term in Equation 6 would spreads out in a wider ring around the object. By spatially filtering out the in focus twin-image terms, and then propagating the spatially-filtered field a distance of $2z_2$ back to the original object plane, the twin-image term can be greatly suppressed without significantly corrupting the object term. This process can be improved further with multiple propagations back and forth between the object and twin image planes, enforcing the spatial filter at the twin image plane each time. For this approach to be successful, the objects must be relatively sparse such that the twin image from one object does not significantly overlap with the image of another nearby object.

Another approach to suppress the twin-image term for sparse samples is shown in Figure 2(b), where PSR with sparse reconstruction regularization demonstrates ability to suppress the twin-image term [18]. Compared to the iterative filtering algorithm, the sparse reconstruction regularization method is more computationally intensive. However, for larger objects, the iterative filtering algorithm could corrupt the object term, resulting in poorer performance compared to the sparse reconstruction regularization method.

When the sample is not sparse, twin image artifacts can be removed by phase recovery techniques that rely on multiple raw frames, either with different z_2 distances [33] where two holograms captured at two different distances are used to iteratively retrieve phase information, or with different wavelengths [34], where wavelength scanning enables pixel super-resolution along with phase recovery. Recently, a physics-driven deep learning based technique was used to suppress the twin-image term in lensless holographic microscopy as well [35].

Besides twin image noise, there are other works on noise minimization in lensless holographic microscopy. For example, fractional Fourier processing is used to remove intensity reconstruction background noise [36]. Other methods of dealing with Gaussian noise have also been recently described, including approaches that use a Wirtinger gradient descent optimization, a common solver used in ptychographic methods [37]. For low-contrast biological samples, one method using an optical phase mask in the light path enabled improved resolution of holographic reconstructions [38]. Neural networks to address image denoising have also been implemented and showed success [39].

2.5 Sample delivery in LHM

As shown in Fig. 1, samples are placed in between the image sensor and light source. Samples can either be stained, labelled, or label-free. In biomedical research and clinical pathology, staining is done by using a dye which stains certain components of a tissue or cells. Clinical pathologists use this method extensively to look at cell morphology, but the staining procedure often uses chemicals and may take some time to perform, delaying procedures like margin analysis during surgical tumor resections. Labelling of tissues or cells typically refers to antibody-mediated labelling, where only a single protein of interest is labelled, typically with a antibody-congugated fluorescent molecule or molecule that can eventually be stained for brightfield visualization. This enables identification of specific cell subtypes in samples, but can be expensive and relies on antibody binding affinities and dynamics to function properly. Label-free refers to a tissue that has been neither stained nor labelled. This type of tissue is translucent in conventional microscopes, but phase imaging still produces useful information about the sample, making LHM one of the few imaging techniques that can effectively use label-free tissues and cells. However, LHM can also be used to image stained and labelled (but non-fluorescent) samples, making this technique quite versatile when imaging biological samples.

Depending on the form of the sample that must be imaged in LHM, different methods can be used to deliver the sample into the light path for amplitude and phase imaging. At its simplest, microscope slides can be used to prepare static or dried unlabelled, labelled, or stained samples [40, 41]. For samples which involve cells dynamically moving in suspension, simple microfluidic chips are utilized for sample delivery [19], on-chip cytometry [20], and automated cell counting [22]. These on-chip methods can also perform 4D (space and time) object tracking [42–44], including tracking of micro-swimmers [21]. In both slide-based and on-chip delivery methods, phase and amplitude reconstructions can be obtained with the appropriate hologram capture protocols.

Other considerations that may affect the hologram include scattering, absorption, and polarization caused by sample-reference interaction. The transparent nature of the slide or chip means that light scattering is caused only by the sample, rather than the delivery method. Absorption typically begins to be a problem only in thick samples, where excessive scattering and high absorption due to the density of the sample work together to degrade information contained in a hologram. For these cases, tissue clearing, where opaque and highly absorptive components of the tissue are chemically removed, or additional hologram capture angles have been shown to enable 3D tissue reconstruction [45–47].

2.6 Deep learning and machine learning approaches

In recent years, deep learning and machine learning algorithms have been coupled with LHM techniques with increasing frequency and in an increasing number of ways. Nearly all of these approaches use a type of network called a convolutional neural network or CNN to perform image processing. This type of network performs convolution operations across input images. Like all neural networks, as data passes through it, the network self optimizes to reproduce a training dataset assembled by a human operator. CNNs have been used in LHM for focus prediction and autofocus [50–56] and image classification [57,58], among other uses.

One particularly useful network architecture, depicted in Figure 3, is the U-net, which enables the network to output images from either an input image or a set of input images [48, 49]. This has been used for PSR reconstructions of holograms [59], phase reconstructions of holograms [52], virtual staining [60], and more. The advantage of using this approach is that it significantly reduces the computational cost and processing time compared with conventional approaches, and it can be more robust when used for a variety of sample types.

Simple, non-CNN networks and machine learning have also been used with LHM, generally preceeded by some form of image processing to produce a one-dimensional vector of input data containing object image characteristics, similar to principal component analysis. This has been applied to LHM for cell imaging [61] and for nanoparticle agglutination [62].

Complete image processing pipelines have been developed using a combination of neural networks to

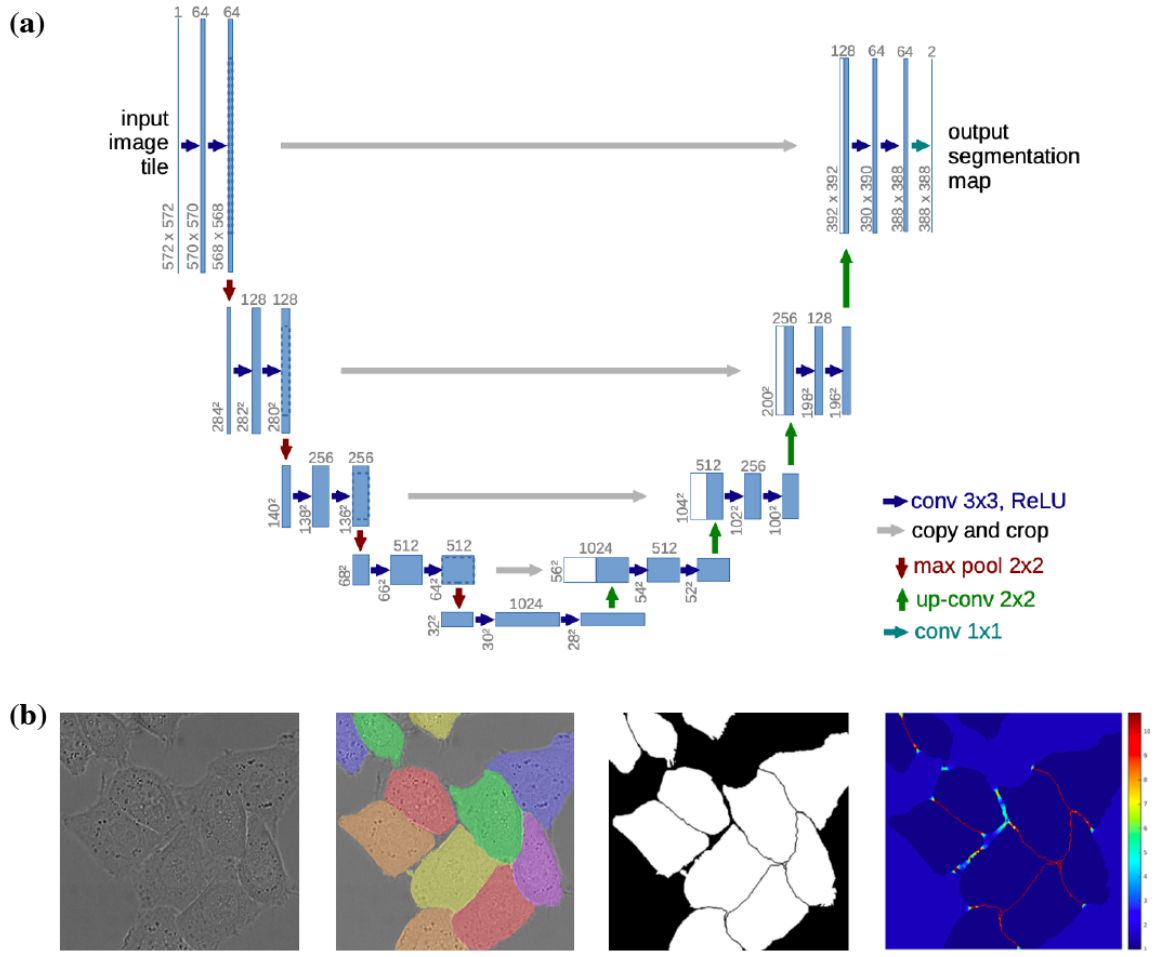

Figure 3: (**a**) U-net architecture commonly used in LHM image processing applications. Blue "conv" arrows denote convolutional layers, which perform a convolution operation using 3 × 3 kernels or filters followed by a ReLU or rectified linear unit activation layer. Red "max pool" arrows denote a max pooling operation which reduces data size. Green "up-conv" arrows denote "up-convolutions" where the data is up-sampled using a sparse transposed kernel matrix. Copy and drop arrows indicate skip connections where information from the contracting or down-sampling side of the network is preserved and passed to the expansive or up-sampling side via concatenation after a center crop. This is necessary for effective network training. (**b**) Image segmentation results of original U-Net architecture. Differential interference contrast (DIC) images of HeLa cells (left) and ground truth segmentation (left center) with U-Net produced segmentation mask (right center and pixel-wise loss (right). Figure reproduced with permission from [48,49].

perform phase unwrapping, reconstruction, and cell metric estimation for cell analysis, showing that deep learning approaches can be applied at each step of an LHM imaging workflow with great success [63]. Many more examples of deep learning in LHM have been demonstrated and will be discussed in the context of the relevant clinical or biomedical application to provide a better sense of the problems these approaches solve and their impact.

2.7 Advantages of LHM

LHM has various advantages over lens-based systems. First, the elimination of objective lenses in LHM decouples resolution from FOV, resulting in large space-bandwidth product. This enables LHM to offer equivalent resolution over hundreds or even thousands times larger FOVs compared to benchtop microscopes [18, 26]. Second, LHM consists of low-cost components that are often either commercial off-the-shelf or fabricated at low cost by 3D printing and laser cutting [19, 62]. Therefore a typical LHM can be built with a few hundred dollars in lab settings. LHMs can be even more cost-effective when manufactured at high volume. Third, unlike typical benchtop microscopes which are bulky and heavy, LHM can be compact and lightweight, making it a suitable solution for field applications [64, 65].

With these advantages, LHM systems have many applications in clinical applications, especially point-of-care and low-resource settings. As a whole, the above advantages empower LHM as a great platform for various applications.

3 Clinical applications of lensless holographic microscopy

LHM has been successfully applied to many clinical applications in recent years. The unique characteristics of LHM enable this technology to be deployed in more locations, including at the point-of-care, at a lower cost than conventional microscopy. LHM also offers additional functionality, and in some ways improves on conventional microscopy. In this section, recent applications of LHM to clinical medicine are explored.

3.1 Pathological analysis of tissues and fluids

For clinical medicine, perhaps no field is more reliant on microscopy than pathology. In recent years, LHM-based devices and techniques have been successfully applied to the imaging of pathological samples for disease diagnosis, including stained and unstained sectioned tissue, thick tissue sections or bulk tissue, cell aspirates, synovial fluid, and cerebrospinal fluid, as described below.

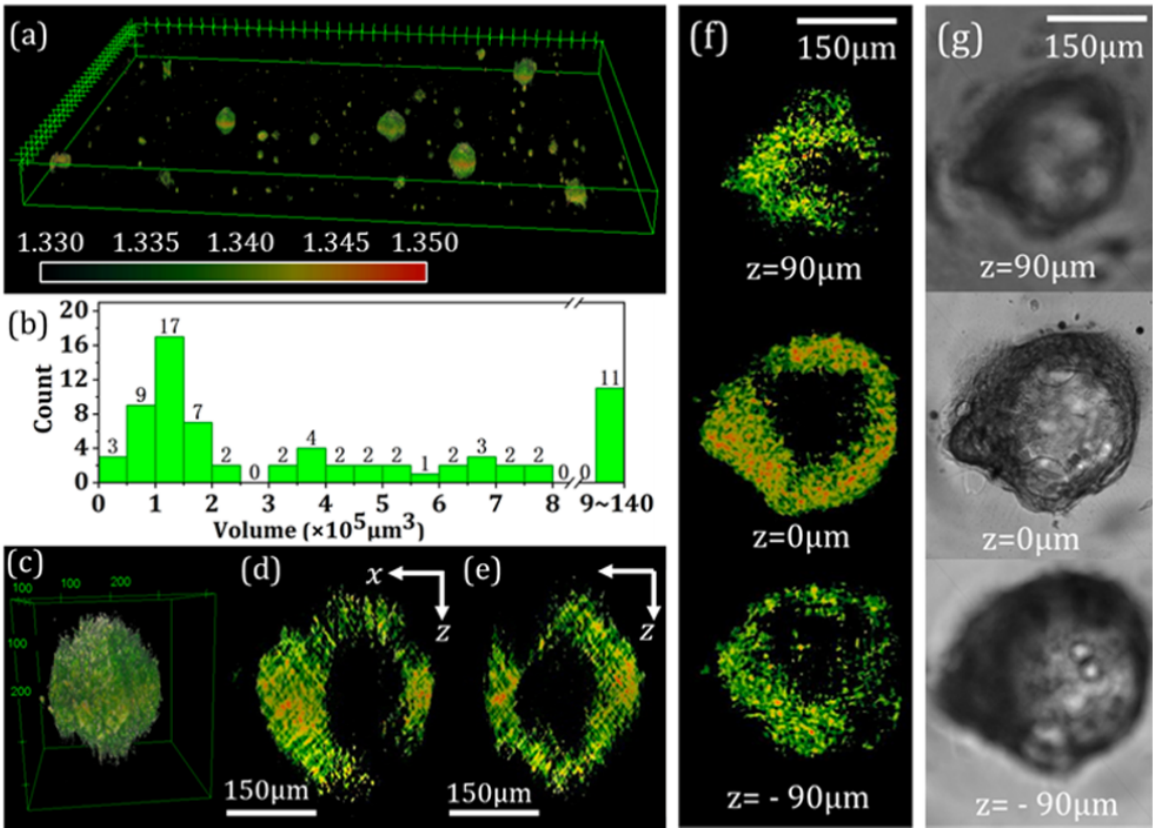

Figure 4: (**a**) Visualization of 3D refractive index reconstructions of salivary gland tumor organoids from a LHM system. (**b**) Volume calculations from 71 analyzed organoids. (**c**) 3D visualization of single organoid and (**d-e**) longitudinal sections of this organoid. (**f**) Cross sections of organoids at various z heights, and (**g**) corresponding bright-field microscope images. Figure reproduced with permission from [46].

Color imaging in pathology is key for sectioned and stained tissue analysis, and there are numerous recent examples of color LHM. Systems incorporating a single-wavelength partially coherent source (similar to what is shown in Fig. 1) and pseudocoloration post-processing are able to generate color images of stained tissue [66]. Recently, multiple wavelength LHM systems that operate in red, green, and blue domains have shown promise in the reconstruction of color images from stained tissue. Additional wavelengths can be used to reduce color error, but three are sufficient to produce accurate images of stained

pathology slides since human eyes also rely on three types of color sensors [67]. Novel computational denoising algorithms have helped to significantly improve reconstructed image quality and color accuracy of bone marrow smear samples with this type of LHM configuration [68]. Deep learning methods have also been developed to produce color pathological images from LHM systems. One method combined a three-wavelength LHM configuration with deep learning to reduce phase artifacts and balance and combine color into a final image [69]. In one study, pseudocolored images were generated with deep learning from phase reconstructions of LHM holograms that closely mimic a number of stains including H&E stain, Jones' stain, and Masson's trichrome for unstained skin, kidney, and liver tissue respectively [60]. Another deep learning coloration method used simple greyscale images from a single green 550 nm wavelength to generate color images of H&E stained samples [70].

Several algorithmic approaches have been developed to aid in data volume reduction and LHM image processing and hologram reconstruction. For example, a phase retrieval algorithm that enables reconstructions with only two z-height holograms has been demonstrated for stained and unstained samples [71]. This simplifies the data acquisition process usually required for other multi-height phase retrieval methods. Image quality and resolution of kidney and intestine pathological slides can be improved significantly by background noise removal, image registration of multi-height and sample scanning holograms, and twin image elimination through multi-height phase retrieval and a quasi-3D reconstruction technique [72]. Novel PSR algorithms have been shown to reduce data volume and even achieve 780 nm resolution in intestine pathological slides [73]. Other computational approaches perform autofocusing for amplitude and phase reconstructions of holograms, either by algorithmic approaches [74] or deep learning approaches [51, 52] which have enabled fast autofocusing for Papanicolaou smear, stained lung tissue, and breast tissue. These deep learning approaches can also produce phase images from holograms since they used phase information from a multi-height phase recovery approach to train the deep learning algorithm, similar to dedicated phase recovery neural networks [75]. A novel deep learning network termed a Fourier Imager Network incorporates Fourier transforms and has been shown to reconstruct phase and amplitude holograms with superior generalization for pathological tissue reconstructions of tissue outside of the training dataset of lung tissue (prostate, salivary gland, and pap smear samples) [76]. Finally, deep learning has shown the capability to produce superresolution images from low-resolution hologram reconstructions to improve pap smear and lung tissue section image resolution without extensive computational costs [77]. Faster data processing times enabled by algorithms such as these can enable immediate diagnostic results. When paired with the POC-nature of lensfree imaging hardware, fast computational processing can lead to significantly better patient outcomes in time-sensitive situations, such as for sepsis diagnosis, during surgery, or for screening in a rural clinic, where patient followup visits are burdensome due to long travel distances.

One of the most compelling applications of LHM in this field is in the 3D imaging of bulk tissue, without the need for staining or sectioning. Since the 3D information of a sample is preserved by LHM holograms, LHM can fully reconstruct 3D samples and provides a significant improvement on conventional microscopy, enabling the imaging of tumors or tissue without the distortions or time and labor cost created by sectioning and staining. Figure 4 shows a 3D reconstruction of a salivary gland tumor organoid made possible by LHM [46]. This technique collects 61 holograms using on-axis and off-axis LED sources such that the light field propagates at a variety of axial and rotational angles towards the sample. Using a modified 3D form of the angular spectrum method described in section 2.2 and the Fourier diffraction theorem, researchers were able to reconstruct the 3D refractive index of the object in a method not dissimilar from tomography. While this does not enable imaging of microstructures or individual cells and cell assemblies, it nevertheless shows that 3D information can be obtained from unprocessed bulk tissue, which would be helpful for clinicians wishing to understand tumor morphology to differentiate various tumor types and staging in different cancers, even during surgery. A similar technique used to image prostatic RWPE1 organoids achieved mesoscopic resolution with the ability to resolve single cells if they are separated from the larger organoid structures [47]. True cellular-level resolution in 3D LHM imaging has been achieved for thick samples (200 μm) of mouse brain [45]. These samples had to be cleared with the CLARITY method and underwent DAB staining to visualize neurons, but 2D reconstructions using

a single LED source and multi-height holograms could be produced at any plane in the tissue.
The 3D imaging capability of LHM makes it especially suitable for the imaging of fluids or aspirates of cells collected in clinical settings. LHM configurations have been successfully applied to suspensions of cells in solution [78]. The insertion of a polarization generator or filter between the light source and sample and a polarization state analyzer or second filter between the sample and image sensor of a LHM setup enables the microscope to image polarization-state sensitive samples. The most clinically relevant use of this setup is to image synovial fluid for detection of gout, whose crystals exhibit negative birefringence under conventional polarization microscopy imaging conditions. The polarization-specific characteristics of needle-shaped monosodium urate (MSU) crystals from gout and oxaloacetate crystals found in urine have been successfully imaged by LHM using a linearly polarized source [79] and circularly polarized source [80] with psuedocoloring to produce a recognizable color image. Additionally, MSU crystals imaged with left-hand circularly polarized light produced holograms that have been colored using a deep learning algorithm so as to quantify polarization state changes in these samples [81]. Urinalysis has been performed using a single-source LHM system to detect and track *Trichomonas vaginalis* in urine [82]. A novel reconstruction method termed adaptive sparse reconstruction, which estimates a point spread function directly from data to perform hologram reconstruction, was shown to image urine with blood cells, crystals, and casts [83]. A recent translational study of LHM in urinalysis with urine phantoms showed that it was sensitive to hematuria and pyuria, correlating strongly to hemocytometer measurements of the same samples by detecting blood cells, bacteria, crystals, and casts [84]. Cerebrospinal fluid analysis using LHM for diagnosis of meningitis has been successfully demonstrated as well, with an LHM configuration that imaged erythrocytes and leukocytes in 215 samples [85]. This device also implemented automated cell counting, which enabled it to achieve 100% sensitivity and 86% specificity compared to confirmed diagnostics, which can help eliminate human error in meningitis diagnosis.
A unique application of LHM in pathology is the ex-vivo analysis of tissues for anatomical research. One LHM system paired acoustic and electromagnetic waves into a single imaging experiment, where a pulsed laser source captured holograms at specific points on a sound wave as it passed through an ex-vivo tympanic ring and tympanic membrane [86]. Two wavelengths were used to map the surface height of the sample interferometrically. This application is unlikely to be performed in a clinical setting as an intervention or used as a treatment, but is nonetheless relevant to pathological biomedical research so is included here.
For pathological imaging, LHM has already shown extensive results replicating and even improving on images achieved with conventional microscopy. The large space bandwidth product enables LHM to function particularly well when looking for disease pathology which may only be present in a small portion of a very large tissue section, as is sometimes the case in cancer pathology. LHM is generally incompatible with fluorescence microscopy, which is also used in biomedical research, due to the incoherent nature of fluorescent imaging. However, other labels such as nanoparticles are often just as effective, and serve as coherent scattering labels [20]. Recently, lensfree (non-holographic) fluorescent microscopy has been demonstrated using a similar in-line system to what is used in other LHM methods but that typically has lower resolution than its holographic counterparts (8.77 μm) [87], due to the lack of interference between the excitation and emitted object waves, which prevents high-resolution reconstruction. However, research is underway to improve this and this could enable lensless fluorescent imaging in the future.
LHM emerges as a superior technique for pathology in the imaging of 3D samples. While 3D reconstructions of thick, unprocessed tissue with cellular-level resolution have not yet been achieved, various LHM imaging techniques have achieved either bulk, unprocessed tissue reconstruction or cellular resolution of processed tissues separately. This is due to a current limitation in LHM where phase modulations to the incident field created by tissues composed of cells, fluids, and extracellular matrix generate too much interference or too little light penetration to effectively reconstruct images from bulk tissues. However, LHM has achieved cellular resolution of 3D samples when cells are dispersed in a 3D medium, as we discuss in the following section, showing that LHM may be on the cusp of achieving high-resolution 3D unprocessed tissue imaging in the near future.

3.2 Cytometric analysis of cells and blood

Cytometry and hemocytometry applications of LHM have been quite common in recent years. For cells floating in fluid such as blood, no other imaging technique can retain information at any focal plane in 3D as efficiently as LHM, making this application an obvious choice for researchers to investigate. Additionally, hematological samples are highly relevant to clinical medicine through hematology, oncology, infectious disease, and immunological biomedical research. These are convenient samples for benchmarking studies of novel LHM configurations due to their availability to researchers. As a result, many recent technological advances in LHM include some form of hematological analysis. For image processing and hologram reconstruction, hematological samples or cell suspensions satisfy a sparsity assumption that can be leveraged to computationally remove twin-image artifacts [18]. Alternatively, some novel methods have been able to remove twin image artifacts through novel hardware configurations that include two light sources, one of which is off axis [88].

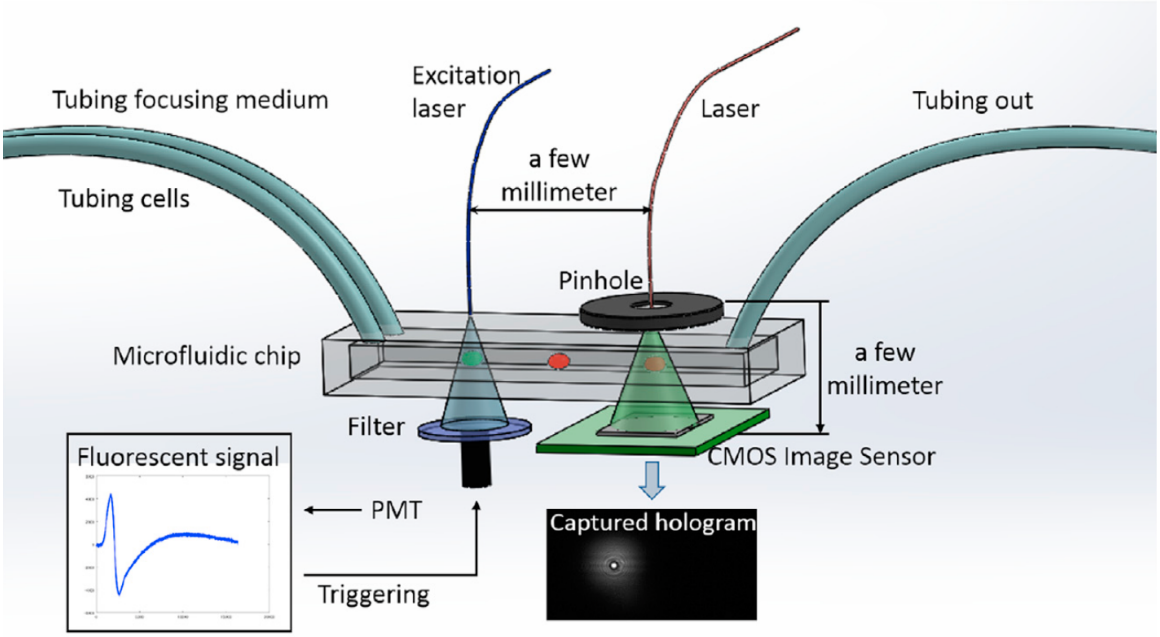

Figure 5: Schematic of an on-chip LHM cytometer with an example of a fluorescent signal and a hologram measured from a single cell as it flows through the chip. This system uses fluorescent signal detection to trigger hologram acquisition and it uses cell characteristics extracted from holographic reconstructions as inputs to a machine learning algorithm to classify immune cells into three leukocyte types: granulocytes, monocytes, and lymphocytes. Figure reproduced with permission from [89].

Portable LHM configurations have become more robust and powerful in recent years. 3D printed designs enable cost-effective, point-of-care (POC) implementation in sizes as small as 55 mm × 55 mm × 40.5 mm (W × L × H) [90] to image buccal swabs and blood smears [91]. The replacement of a pinhole filter with a cone-shaped optical fiber tip has been shown to be viable in portable and non-portable LHM configurations for imaging blood smear samples, improving device stability and robustness compared to a pinhole filter [92, 93]. A benchtop holographic point-source configuration has been described for buccal swab and blood smear imaging which also achieves improved device stability (and therefore improved portability) by using off-axis light to illuminate a photopolymer holographic film that encodes a transmission hologram of a point source [94].
Computational techniques, like PSR, have been applied to cytometric samples as well. PSR has been demostrated in a portable LHM setup for platelet imaging with 1.55 μm lateral resolution through a stationary light source and shifting pinhole [95]. Other pixel super resolution techniques have been effectively implemented to improve single-cell resolution in benchtop setups. Arrays of diodes have been understood for over a decade to be effective for this task [96], and additional processing using algorithms for motion estimation have recently enabled pixel super resolution to be performed on free-floating sam-

ples undergoing Brownian motion [97]. Gradient-descent phase retrieval methods have been shown to resolve twin-image artifacts and achieve a depth resolution of 50 nm in red blood cell images with a single illumination source [98], while additional registration steps have been tested to determine precise z-positions of holograms for more effective phase retrieval [99].

LHM's ability to image cells in suspension due to its resolution, FOV, and 3D imaging characteristics enables it to perform superior motility analyses of sperm cells compared to conventional methods. Early methods using multi-illumination and multi-wavelength conditions tracked sperm in 3D using on-chip integration and revealed sperm cells travelling in helical trajectories [21]. However, a simple single-illumination and single-wavelength LHM can also perform 3D imaging of sperm cells by employing more standard reconstruction and focusing techniques [78, 95]. A technique called MISHELF (multi-illumination single-holographic-exposure lensless Fresnel) microscopy, which uses three distinct wavelengths that are combined before sample illumination and a novel fast converging algorithm for image reconstruction, similarly tracked sperm in 2D and 3D for motility and morphological analysis [100–102].

Cytometric samples can be easily integrated into LHM systems with on-chip processes to further expand device functionality. As in conventional flow cytometers, cell sorting and counting algorithms are typically part of these modern LHM systems. Simple configurations with a single illumination source have captured intensity reconstructions of diluted cells flowing through an S-channel microfluidic chip and have used a thresholding-based image segmentation approach to count cells with reasonable success [103]. A Fourier domain-based classification algorithm has recently been shown in a similar on-chip LHM setup with a straight channel for classifying white blood cells into three subtypes using a raw hologram without image reconstruction [104]. Other methods use deep learning algorithms to count, classify, and even distinguish different cell populations [105, 106]. This approach has been translated into a 3D printed device [107]. These counting methods have shown success when working with multi-height phase reconstructions and with intensity reconstructions. Moving closer to the functionality of modern flow cytometers, one LHM-based method used nanoparticles bound to target cells to increase scattering and enhance LHM imaging performance [20]. The specific plasmon resonance characteristics of the particles allowed for the classification of immune cell populations based on the cell's CD4 and CD8 expression. Magnetic beads functionalized for specific cell detection have been used on-chip to detect target cells in blood on-chip by applying a periodic magnetic field which enables a simple LHM system to distinguish rare cells in blood [108]. This is relevant for diagnosis of leukemia and other cancers. One particularly sophisticated method combines on-chip microfluidic cell separation, automated cell counting, and fluorescence detection in a single platform to distinguish 3 different types of leukocytes [89, 109]. Figure 5 shows a schematic of this method, in which cells flow through a microfluidic chip where a first fluorescence signal is detected and recorded, then used to trigger acquisition of a hologram after the cell has moved into the holographic imaging region of the chip [89]. This pairs high-resolution imaging of a cell with its fluorescence signature for every cell that passes through the microfluidic chip, a new feature found in expensive modern flow cytometers, but replicated here in a low cost, compact, and portable platform.

LHM has several advantages over conventional methods of cytometric analysis involving conventional microscopy and even flow cytometry. Firstly, LHM can easily achieve the same resolution and reproduce the same images for these samples as conventional microscopy. This enables LHM to be used in low-resource, POC, and large hospital settings where hemotological analysis would be instrumental to clinical decision making. LHM also preserves the 3D information in a sample, allowing a technician to perform fewer sample processing steps and track cells in real-time for clinical information. However, this does come at the cost of some training on the particular LHM system. Additionally, LHM systems are more sensitive to dust and impurities in the sample in question, which can place additional burden on a trained technician in the sample processing steps. On-chip functionality also enables LHM to replace other techniques like flow cytometry for cell expression analysis and cell counting in a low cost and portable device. One LHM system, NaviCell, has reached the commercial stage and has shown high accuracy when compared with conventional, dye-based hemocytometers, and can even perform cell viability testing functions (see Section 4.2) [110]. Another commercial system, Cellytics, has shown effective cell sorting of

blood cells and cancer cells when images produced with this system are passed through a deep learning classification algorithm [58]. These devices successfully combine on-chip functionality, cell counting and sorting algorithms, and the inherent 3D imaging characteristics of LHM. The advances of LHM devices in pathology demonstrated in recent years illuminates LHM as a compelling emerging technology in clinical cytometric analysis which requires more clinical study.

3.3 Infectious disease monitoring and diagnosis

LHM techniques have a wide variety of configurations and coupled methodologies when applied to infectious disease monitoring and diagnosis. Typically, traditional infectious disease diagnosis involves microscopic visualization of individual infectious particles such as malaria or parasites, visualization of colony-forming units (CFUs) or plaque-forming units (PFUs) in bacterial or viral culture, measurement of viral or bacterial load like what is done in lateral flow assays (LFAs) or polymerase chain reaction (PCR) analysis, or a combination of these techniques depending on the specific disease. LHM has been tested successfully for each of these detection methodologies.

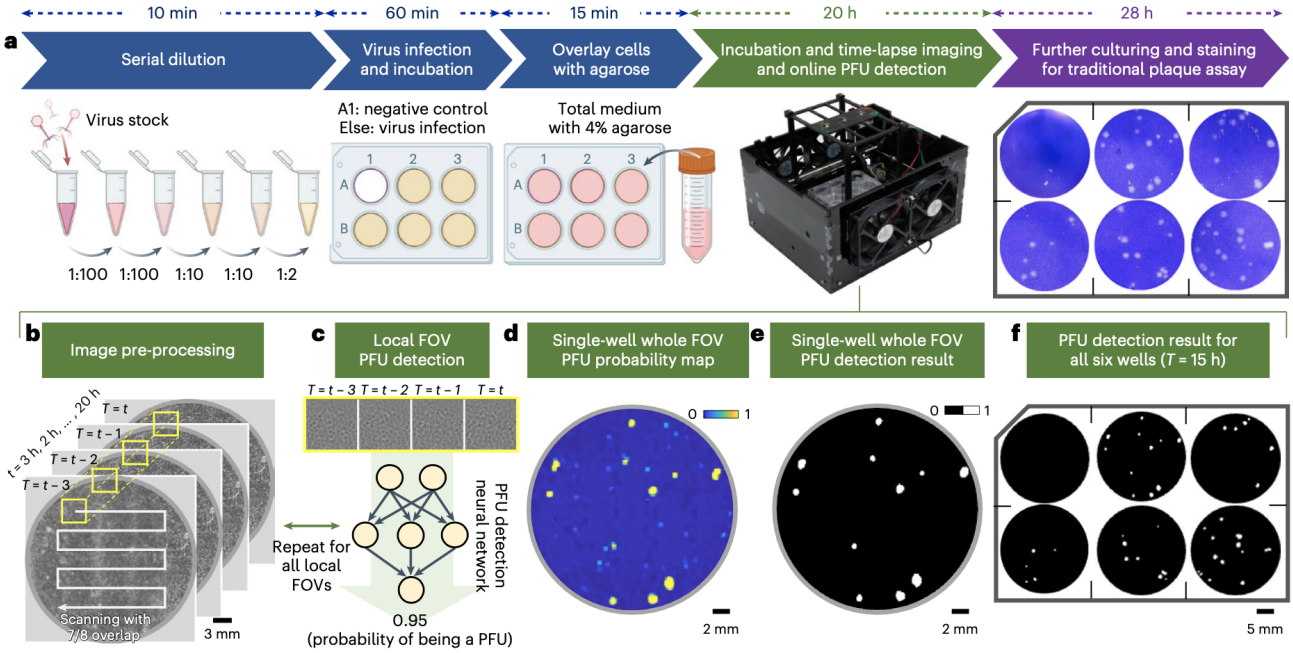

Figure 6: Workflow for a LHM-based system to quantify viral plaques. (**a**) Sample preparation for plaque assay, with a traditional plaque assay shown at the end. (**b-f**) LHM imaging and live viral plaque quantification workflow that is performed before the traditional quantification assay. (**b**) Whole-well holograms are captured for different time points. (**c**) A DenseNet-based [111] neural network is used to create (**d**) a probability map for plaque-forming units (PFUs) for each hologram by scanning across the hologram spatially and temporally. (**e**) PFU detection performed through application of a threshold of 0.5 to the probability map. (**f**) Result of processing of whole 6-well plate. This method yielded an assay with a 10-fold higher dynamic range with reduced incubation times than conventional approaches without the need for staining. Figure reproduced with permission from [112].

Direct visualization of individual bacteria with LHM imaging has been achieved in a variety of configurations and contexts. The simplest LHM systems are capable of imaging disperse samples of microorganisms. However, because of their simplicity, these systems can suffer from poor resolution limits, which makes visualizing organisms any smaller than large bacteria challenging [113]. Fundamentally, LHM resolution, under optimal configurations based on the sensor, wavelength of light used, and source-sample-sensor distances, is limited by the sensor's pixel size [114]. Under optimal configurations, *Schistosoma haematobium* eggs, parasitic eggs present in stool and urine of infected individuals, and *t. vaginalis* parasites have be imaged [82]. 3D motility of *t. vaginalis* has been used as an endogenous biomarker for automated biosensing of this parasite in dense blood or cerebrospinal fluid with an LHM system that scans across a capillary tube containing 3.2 mL of fluid [115]. A three-wavelength LHM configuration has been

shown to provide micrometer resolution to image *Giardia duodenalis* cysts in contaminated water [116]. Tightly tuned LHM configurations enable detection of parasites or even large bacteria, but typically not smaller pathogens. Several techniques have attempted to split the reference and sample waves to achieve higher resolution, a technique which produces global interference fringes similar to Michelson interferometer-like digital holographic microscope configurations. One LHM which used two small GRIN lenses to do this still had difficulty resolving bacteria like *Bacilis subtilis* [117]. This reference and sample wave splitting has also been achieved by collecting holograms from a reflected field created by a step-down chip design [118], and by passing the source wave through a prism with two diffraction gratings which direct a single diffraction order each towards the image sensor, with one beam passing through the sample and the other reference beam propagating unaffected [119].

PSR techniques, which computationally reduce pixel size, are therefore often necessary to achieve the resolution required to visualize pathogens directly. One configuration used an LED array to achieve PSR-based imaging of malaria (*Plasmodium falciparum*) parasites in an LHM system [96]. A similar PSR technique coupled with on-chip immune-based immobilization of HSV-1 and HSV-2 viruses enabled the visualization and sizing of these small viral particles directly [120]. A simplification of typical LHM systems through the substitution of a cone-shaped optical fiber tip instead of a pinhole filter in a single-source LHM setup also enabled direct visualization of microorganisms in pond water [93].

Other, even more creative (although potentially difficult to implement translationally) methods have been explored to improve LHM imaging for pathogens. The deposition of polyethylene glycol onto immobilized adenovirus and influenza A virus created small nanolenses which enabled visualization of the virus [121]. Ultrasonic wave propagation has been shown to similarly produce nanolenses around nanoparticles, rendering them detectable in solution through LHM, which could theoretically be possible with small pathogens [122].

When performing bacterial or viral culture for diagnosis of infectious disease, often time is the main cost. LHM presents some compelling methods that reduce the time it takes to process these types of samples, and even reduces the sample processing complexity. Since effective imaging of bacterial and viral culture involves quantification of colonies or plaques rather than single microbes, high resolution techniques do not need to be used. This allows for the use of simple LHM imaging configurations that permit use within incubators, or the incorporation of additional sample handling and environmental control components within the LHM microscope itself. Recent examples of LHM used for this application include bacterial culture imaging, where a moving stage and heating plate are introduced into the microscope to take scanning images of an entire bacterial culture plate [123]. Stitched images were paired with a deep learning algorithm so that bacterial growth was detectable in only 3 hours, and classification among 3 different disease-causing bacterial strains was reliable within 7–12 hours. Viral plaques have also been quantified using a very similar setup (Figure 6), which combines a simple LHM imaging configuration with in-microscope temperature control and deep learning to quantify plaque-forming units (PFUs) for viral cultures of VSV, HSV-1, and EMCV more rapidly than conventional approaches and without the need for staining [112]. LHM has also been used to visualize and quantify *Staphylococcus aureus* phage plaque growth in nearly half the time of conventional assays, which is important for the development of novel antibacterial targeted phage therapeutics [124].

LHM has also been applied as a component of immunoassays for sensing of pathogens. These systems generally image infectious particles indirectly through a sandwich assay, where one antibody is used to fix the target to a surface, and a second antibody is conjugated to some reporter molecule or microparticle. Immunoassays have been coupled with LHM in several ways. One unique method immobilized *Staphylococcus aureus* bacteria onto a contact lens surface, using 5 μm polystyrene microspheres to visualize bound bacteria, and accounted for surface topology with computational techniques to achieve a detection limit of 16.3 colony-forming units (cfu) / μL [125]. Agglutination assays, discussed in more detail in Section 3.4, have also been shown to detect infectious diseases indirectly. Using a single illumination source, 2 μm polystyrene spheres can be resolved [53]. Tracking the agglutination of these particles in response to HSV-1 with LHM enabled a limit of detection of 5 HSV-1 viral copies/μL to be achieved. In this method, a deep learning algorithm was used to perform autofocusing and phase recovery of par-

ticle clusters. Deep learning and particle agglutination have been combined in a LHM-based portable COVID-19 assay as well, enabling detection of SARS-CoV-2 virus at concentrations as low as $1.27{\cdot}10^3$ copies/mL while using deep learning to accommodate cellular debris in LHM reconstructions [57]. This limit of detection is similar to that in polymerase chain reaction (PCR) tests, but is simpler and faster to perform than PCR.

Culture and PFU analysis is the most commonly used method to determine the appropriate antibiotic to use for treatment in an inpatient clinical scenario. Some diseases are diagnosed through a patient's history or physical exam findings, but sometimes empirical antibiotic treatment is started without fully knowing which bacteria is present due to the time it takes for a culture to grow. This delay can be a contributing factor for the development of antibiotic-resistant bacteria. A better approach could be provided through LHM, since these methods can detect and quantify infectious diseases much faster than traditional methods, without the need for sample processing, and in POC settings. The FOV, high resolution, and component simplicity of LHM enables this method to be used effectively for clinical infectious disease diagnosis. Some of the typical limitations of LHM continue to be disadvantageous in this application, including sensitivity to dust and debris, and computational load, but several of the above referenced studies have shown that computational techniques and deep learning methods are starting to resolve these limitations and make LHM a compelling approach in this field.

3.4 Molecular diagnosis and biosensing

As modern medicine advances, biomarkers for disease are becoming important areas of research. Current widespread methods of performing molecular biosensing are the enzyme-linked immunosorbent assay (ELISA), LFAs, PCR, and others. Each of these approaches has their own advantages and drawbacks—for example, PCR and ELISA are both known to be sensitive tests with very low limits of detection, but they require technician training to perform and often are unavailable in POC settings due to system bulk and infrastructure requirements. LFAs are ubiquitous, as they can be utilized in virtually any environment and are inexpensive to manufacture, however they are not very sensitive, requiring a high target concentration to yield a positive test, and are not quantitative. LHM-based techniques have recently attempted to combine a very low limit of detection with POC utilization in a number of ways to detect biomolecules.

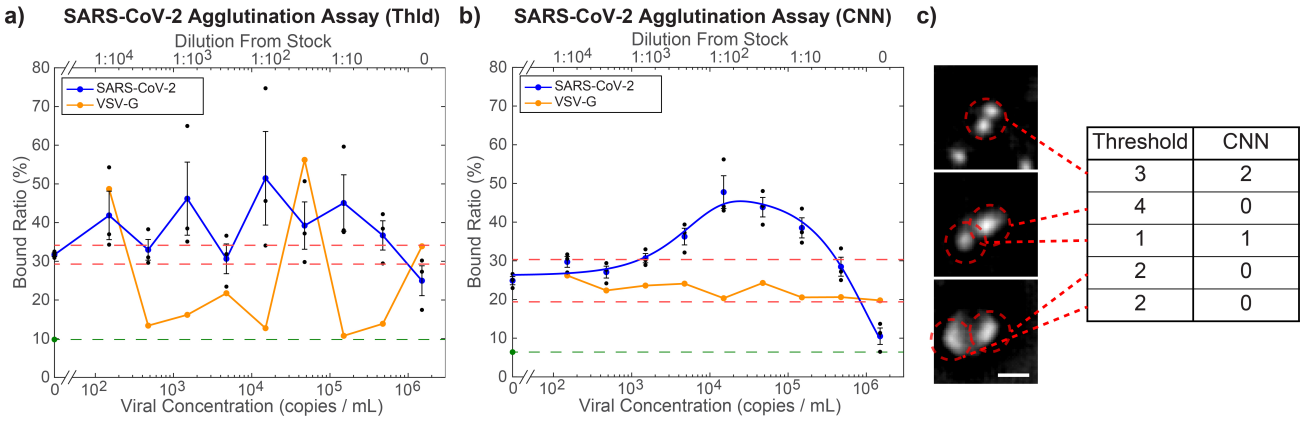

Figure 7: Quantification results from a LHM biosensor used to image an agglutination assay for the detection of SARS-CoV-2 pseudovirus. (**a-b**) Analysis of pixel super-resolved hologram reconstructions of agglutinated microparticles mixed with viral particles and cell debris using either (**a**) a thresholding-based image segmentation approach or (**b**) a residual CNN-based feature classification approach. Vesicular stomatitis virus G (VSV-G) served as a negative control and three times the standard deviation of variation of the zero-concentration point was used to calculate a limit-of-detection threshold (red dashed lines) (**c**) The CNN performed better on feature classification than the thresholding approach as it was able to distinguish debris in the sample from agglutinated particles. This enabled the detection and quantification of viral particles at a concentration as low as $1.27{\cdot}10^3$ copies/mL. Figure reproduced with permission from [57].

As mentioned in Section 3.3, agglutination assays present a powerful sensing methodology when combined with LHM. In an agglutination assay, microparticles or nanoparticles are functionalized with an

antibody or capture molecule to detect a specific target biomolecule or cellular surface marker. In the presence of this target, the particles will sandwich the target, resulting in agglutination of particles. At high enough concentrations, particle aggregates can even become visible with the naked eye. So long as a system exists to quantify this agglutination, the particles can be functionalized to detect virtually any biomolecule. LHM's large FOV and high resolution enables it to detect very subtle changes in particle agglutination as target concentration increases, enabling a much more sensitive readout of particle agglutination assays. Figure 7 shows results from an agglutination based biosensor for SARS-CoV-2 virus [57]. In this configuration, also discussed in Section 3.3, PSR was performed using a high-speed LED array to limit blur from Brownian motion, and deep learning was implemented to quantify agglutination while accounting for debris in the large FOV. This enabled a limit of detection on the same order as PCR. Additionally, this method was portable and achieved a readout of results in less than 3 hrs in POC settings, showing effective combination of the sensitivity of PCR and portability. This same PSR LHM system has also been used to detect biomolecules like interferon-γ, a pro-inflammatory molecule present in sepsis [19]. In non-PSR LHM configurations, a detection method for HSV-1 has already been discussed in Section 3.3, but the deep learning-based autofocus and phase reconstruction can easily be translated to any biomolecule assay by changing particle functionalization [53]. Another LHM agglutination assay was unable to resolve individual nanoparticles, but could detect the agglutination of large enough particle clusters which, when coupled with a deep learning quantification algorithm, enabled c-reactive protein (CRP) concentrations as low as 0.5 μg/mL and as high as 500 μg/mL to be detected, relevant for heart failure and inflammation [62]. DNA molecules have also been sensed with magnetic particles, albeit not through agglutination, but rather a sandwich assay where magnetic particles acted as reporters to visualize target DNA linkage using LHM [126]. This resulted in the detection of DNA concentrations down to 10 pM.

LHM biosensors are an emerging field that has the potential to have a high impact on the way clinical tests are performed. The portability and imaging characteristics of LHM systems enable a single system to be effectively coupled with microparticles and nanoparticles to indirectly sense the presence of important biomolecules for many diseases. However, these LHM systems still present a typical cost of around $200, and users would need training and access to moderate computational resources. Fortunately, once LHM platform access has been established, individual tests for these systems tend to be on the order of a few cents per test, and deep learning algorithms have been shown to lighten computational load, reducing the cost over time and making LHM an active area of research for novel biosensor platforms. As biomarkers become more important in the diagnosis of neurodegenerative disorders, cancer, and in the development of personalized medicine, LHM technologies can help meet the clinical demand.

4 Use of lens-free holographic microscopy in biomedical research

LHM-based methods have seen increased use in the last five years in the context of biomedical research, impacting clinical medicine and our understanding of disease, treatment, and fundamental biology and medicine. LHM presents a unique and potentially transformative technique that in recent years has enabled researchers to make observations and to answer questions in novel workflows that would otherwise be impossible without LHM. LHM has also been shown to be an alternative to conventional imaging for several applications in biomedical research, and has been implemented into existing workflows seamlessly. In this section, we discuss LHM within the context of biomedical research, focusing on basic science uses of LHM and how LHM can enable these types of research endeavors.

4.1 Live-cell imaging and cell culture analysis

Within the context of biomedical research, perhaps no application is more suited to LHM than live-cell imaging. This type of imaging is widely used for research involving cell growth and cultures, including cancer research, developmental biology, and stem cell biology. The absence of objective lenses in LHM systems means that these systems can operate in a variety of conditions, including high humidity and

warm temperature environments like those inside incubators used to grow and maintain cell cultures. Figure 8 shows results from one particular system that captured multi-angle holograms to retrieve 3D information from cells as they grew in culture inside an incubator [127, 128]. The frequently captured timecourse reconstructions enabled researchers to discover novel cell-to-matrix and cell-to-cell interaction and migration phenomena, without disturbing or removing cells from the incubator. Simple single-source LHM configurations have tracked and quantified cell growth and cell motility as well, including analysis of neuroblastoma cells in culture [129]. A novel 4-hour ultradian rhythm was discovered through single-source LHM imaging of the dry mass of thousands of cells in culture, which, when coupled with pharmacological interventions to probe different points of the cell cycle, revealed that the rhythm represents a massive degredation and re-synthesis of protein during the cell cycle [130]. Cell cycle tracking of individual cells has been achieved with single-source LHM cofigurations, and the inhibitory effect of actinomysin D on the cell cycle has been observed [131].

To aid in and automate the reconstruction and quantification of LHM holograms, parfocal autofocusing methods have been created, where wave propagation properties and image intensity distribution are used to establish a continuous autofocus condition, similar to a parfocal lens. This approach can continuously monitor growing cells and track the motility of neuroblastoma cells and bacteria [132]. Cell tracking has been automated computationally in another simple LHM configuration, which enabled researchers to compare cell motility for NIH 3T3 cells on substrates of fibronectin and type IV collagen [133]. Deep learning methods have also been used to analyze LHM images of live cell culture, where they perform everything from phase unwrapping for phase retrival to estimation of cell metrics for analysis, processing over 25,000 cells per second [63].

Some samples of cell culture can be quite dense, creating problems for hologram reconstruction. To improve reconstruction under these conditions, several methods have been explored. One multiwavelength LHM system used red, green, and blue LED illumination sources to collect holograms from dense cell cultures [134]. This enables phase retrieval and resolves the twin-image artifact without relying on a sparsity assumption, which allowed researchers to track cell confluence as growth and proliferation occurred. A similar configuration imaged and tracked individual cells as they progressed through the cell cycle and divided, yielding over 2×10^6 measurements [135]. Another compressive sensing approach showed promise as an alternate method to remove this twin-image artifact and was tested for images of cells in culture [14].

LHM can also be used in situations where light must be kept to a minimum to prevent disturbing or harming cell growth. In one such low photon budget application, live glial progenitor cells were imaged successfully in-incubator using as little as 7 μW of illumination power in a simple single-source LHM system [136]. This method was also effective for imaging stained sections of ex-vivo rodent neural tissue. The main advantage of using LHM to monitor and quantify growing cells in culture is its ability to do so in-incubator with minimal sample interference. The compactness, FOV, resolution, and absence of lenses in LHM systems enables them to function well even within this challenging environment. Furthermore, imaging protocols can be automated to continuously monitor samples without sample alteration. The performance of LHM under low photon budget constraints further reduces cell damage that can occur with extensive sample manipulation and conventional imaging. Drawbacks of using LHM such as the density of samples affecting the image quality are being addressed. These factors, combined with the novel workflows developed and the discoveries that have been made using LHM, make LHM a compelling choice for future biomedical research involving live cell culture.

4.2 Pharmacological testing

Biomedical research on pharmaceutical development is important for drug discovery and the initial stages of drug testing before clinical trials. Pharmacological testing, particularly of chemotherapeutic drugs for cancer treatment, has recently begun to benefit from LHM-based imaging and analysis methods. Utilizing the same in-incubator approaches that make LHM ideal for live-cell imaging in culture, LHM also presents an ideal platform for cell viability analysis. This has been accomplished with a single-source LHM setup used to image cultured cells exposed to methyl mercury in a 96-well plate [137]. Other sim-

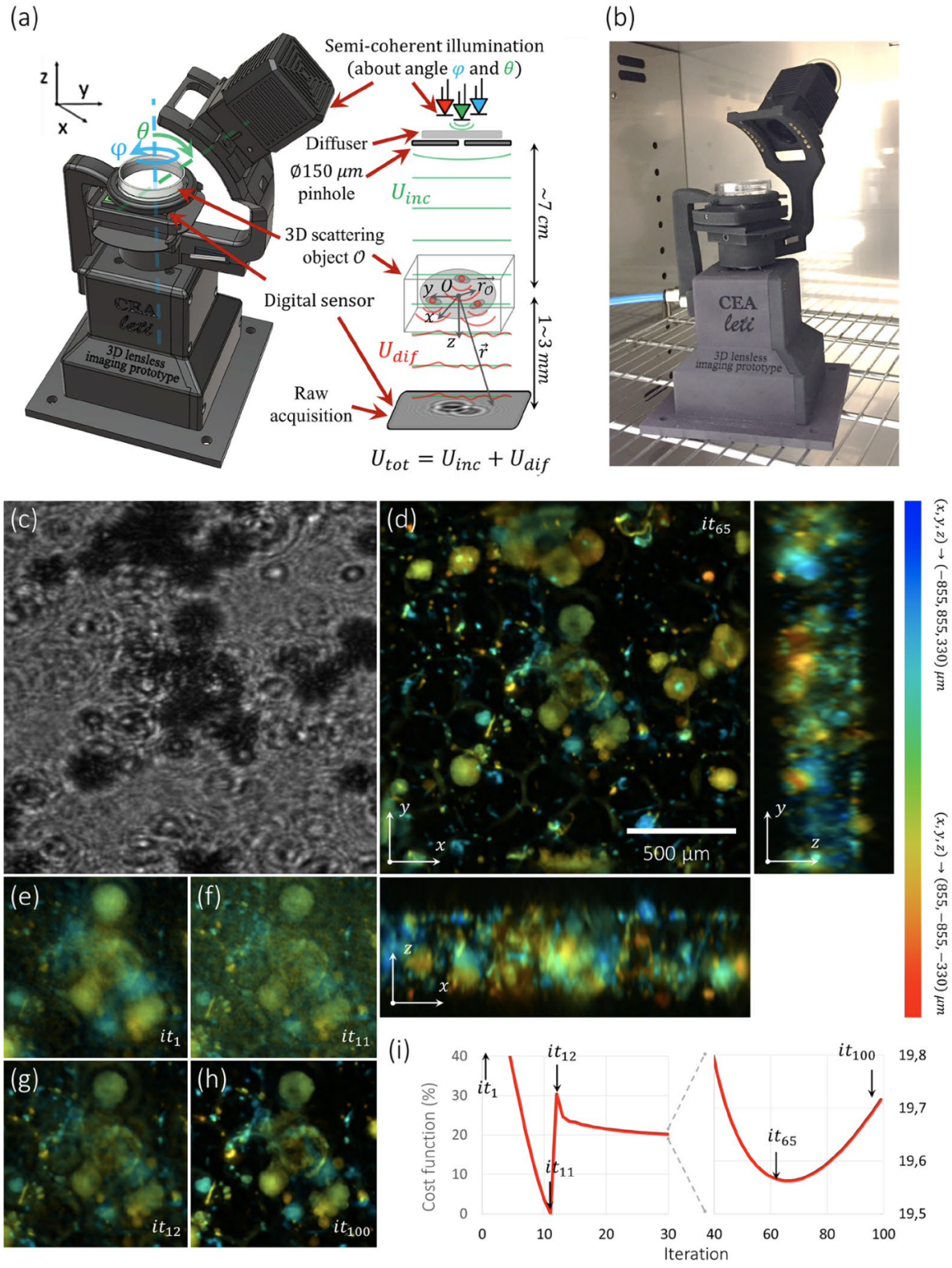

Figure 8: (**a-b**) In-incubator compact LHM device used to reconstruct 3D information from prostatic RWPE-1 cells in culture over time. (**c**) 1 of 31 raw holograms captured with this device and used to perform the 3D reconstruction. (**d**) 3D orthogonal average intensity projection for the reconstructed sample volume where color denotes object depth relative to the plane shown: blue being high, red being low. (**e-h**) Average intensity projections at the data processing iteration shown in the bottom right of each image. Each iteration fills in additional information according to a cost function (shown in **i**). This device was used to discover a new phenomenon regarding cell-to-matrix and cell-to-cell interactions and migrations of growing tumor cell cultures. Figure reproduced with permisssion from [127].

ilar LHM configurations have been used to perform cell viability testing for scraped and suspended cells in solution, enabling viability analysis to be performed on triple negative breast cancer cells exposed to

apoptotic and necrotic drugs with the incorporation of a deep learning algorithm for live/dead cell classification [138]. This bypasses the need for flow cytometry in this type of research. Cell cycle arrest has also been observed through LHM imaging of cells treated with doses of several inhibitory drugs [139]. Another method used fractal geometries of suspended cells with machine learning to classify live and dead MCF-7 cancer cells stained with tryptan blue [61].
Several on-chip methods have also been developed for LHM-based viability analysis. One method simply characterized cells into live and dead populations based on their diameter and refractive index as cells flowed through a microfluidic chip without the need for staining or additional processing [140]. Another on-chip method first placed cells in a paramagnetic medium before applying a magnetic field across a microfluidic chip [141]. Under these conditions, cells will levitate towards the center of the chip, with live cells, being denser than dead ones, moving towards the center more quickly. In-depth image processing was used to detect mouse bone marrow cells and breast cancer cells and determine whether populations of these cells were alive or dead via apoptosis. The previously described commercial LHM cytometer (Section 3.2) is also capable of performing cell viability analysis [110].
Research into the use of LHM for cell viability analysis has resulted in the development of multiple methodologies to assess the effects of novel therapeutics on cells. This has been shown in on-plate, on-chip, and in-suspension analysis methods, which have used stained, or labelled, and unlabelled samples. For this application, superresolution techniques are unnecessary since mammalian cell lines, which are most commonly used for viability analysis, are on the order of tens of microns, making them easily resolvable by most LHM systems. Additionally, LHM is well suited for this application because cells can be analyzed on-plate over time after drug exposure without disturbance.

4.3 Basic biological science

This final category of LHM application is the furthest removed from the clinic, however it is nonetheless important to cover as the dissemination of basic biological discoveries often has transformative effects on translational research and patient treatment in the clinic. To this end, LHM has been used to investigate various basic biological science questions. PSR techniques in LHM have enabled the investigation of microorganisms like *Caenoharbditis elegans* with resolution comparable to a 40× microscope objective [26]. At this resolution, organelles and internal structures of *C. elegans* are visible. PSR in LHM has also been shown to enable reconstruction of multilayer samples by leveraging the 3D information preserved in the holograms [142]. More advanced PSR algorithms have been demonstrated that virtually rotate the pixel layout of a color image sensor to achieve amplitude and phase reconstructions with 350 nm lateral resolution and gigapixel images of *C. elegans* [143]. Additionally, tomographic or 3D reconstructions have been obtained using this LHM setup by capturing angled holograms. Another approach to enhancing LHM resolution for basic biological research involved laterally shifting a sample and capturing multiple holograms, which enhanced the FOV of the image and, through a unique PSR algorithm, resulted in higher resolution in the center of the image and lower resolution around the outer edges with reduced data volume [144]. This approach was used to image the leg of a fly. Other methods of LHM image quality improvement have also been applied to biologically relevant samples. An algorithmic approach with a parameterized sharpening step was able to significantly improve the contrast of LHM images of the head section of a *Drosophila melanogaster* fly [145].
To address drawbacks of conventional biological imaging, several LHM techniques have been developed and tested. For samples where light could impact growing or sensitive samples, imaging must use a low-photon schema. One LHM system managed to produce images of ex-vivo rat neural tissue and live glial progenitor cells with illumination intensity as low as 7 μW (also discusssed in Section 4.1) [136]. Autofocusing methods, whereby an LHM hologram reconstruction distance is selected by scanning through several reconstruction distances and a distance with a local minimum pixel value is selected, enabled effective resolution of paramecium floating in solution and of section of a *D. melanogaster* fly [146]. Finally, to address the computational load that phase retrieval can have on LHM, a subsampled pixel approach has been developed, enabling a 5.5× improvement in video framerate and order of magnitude fewer pixel measurements in the phase imaging of paranema microorganisms [147].

LHM configurations in basic biological applications tend to be fairly simple in their design, consisting of a single illumination source or otherwise employing an array of sources or a moving sample stage to acquire images for PSR. For these applications, high-resolution imaging tends to be the most desirable, and so algorithms that either improve resolution like PSR, aid in focusing like autofocusing algorithms, or improve image quality like contrast enhancement are indispensable. LHM can easily be tuned to operate within the constraints imposed by biological samples, such as low-light conditions, or even (multilayer) cell growth conditions. Additionally, fluorescent imaging, which is generally incompatible with LHM due to its incoherent nature, has been demonstrated which could enable lensless imaging of fluorescently labelled samples using the same in-line configuration used for lensless holographic imaging techniques, albeit with significantly reduced resolution (8.77 μm) [87]. One recently developed lensless imaging method used calcium fluorescence imaging in in-vivo mouse brains and a optical phase mask to track neural activity during running [38].

5 Conclusions and Outlook

In this review, we have discussed a number of key innovations for LHM that enabled its application to many high-impact regimes in clinical medicine and biomedical research. In clinical pathology, LHM benefits from being compact and POC, and can become transformative in this field through 3D imaging of bulk tissues. On-chip functionality is key for LHM's success in cytometric applications. High-resolution LHM configurations are very useful for infectious disease monitoring and for biosensors utilizing micro or nanoscale particles. In biomedical research, LHM enables unique and compelling new workflows through in-incubator continuous monitoring of cell culture and cell viability analyses. Finally in basic biological research, high-resolution LHM and the customizabity of LHM systems is particularly beneficial. Overall, the breadth of computational and deep learning approaches for image processing and quantification have played a major role in LHM's success in these fields.

Several key aspects of imminent LHM research will likely lead to transformative clinical and biological impact. One clear example is to extend the work done with 3D sample imaging, especially for treatment and excision of cancers, which could significantly improve surgical outcomes in cancer patients. Another is the in-incubator approaches for LHM cell culture monitoring. Refining and translating these systems could enable quite novel workflows in biomedical research to answer questions relating the stem cell research and regenerative medicine, as well as infectious disease and pharmacology. The translation of technology into this field is still nascent, with great future potential. The absence of many commercial LHM-based systems in clinics and in laboratories indicates the need for more work in this area.

Other areas of future research will be directed at addressing the common drawbacks of LHM in clinical and biomedical applications, such as LHM's sensitivity to dust or debris in a given sample, the difficulty of reconstructing dense samples without artifacts, and the computational load of LHM, which presents the main barrier for effective POC implementation. Deep learning in particlular seems to be an ever-growing method in LHM applications and can pose some significant advantages for data processing and visualization, as well as some risks. Traditional LHM image reconstruction and quantification is based on physical properties of either light or of the sample. As such, traditional image reconstruction is a physics-based method that can produce accurate images of unexpected outcomes, perhaps of tissue that was not stained correctly but tells us something new or unique cell growth characteristics never observed before. Deep learning, on the other hand, can be unreliable in processing data that is dissimilar from what it was trained on. This is because it optimizes its performance from a limited training set and is unconstrained by physics. The training dataset, therefore, should ideally encompass examples of all possible outcomes. This is nearly impossible to do, so each network will need to generalize to unfamiliar inputs occasionally, in which case it could "hallucinate" and generate reconstructions that are not truly present in the sample. This could be a massive problem in clinical application, so caution is essential.

Some interesting research has been performed on lens-based holographic systems (often referred to as digital holography) that could easily be converted into LHM systems. These systems often place a lens between the sample and the sensor, using the lens to magnify a hologram before recording it. This im-

proves the resolution of the system, but reduces the field of view. Placing the sensor at the focal plane of the objective, along with some PSR and other image improvement techniques would convert these systems to operate lens-free, reducing cost, improving portability, and enabling them to function in a wide range of environmental conditions. Systems like this have been applied to some of the same applications already discussed, such as on-chip leukemia detection [148], red blood cell imaging for anemia diagnosis [149], and malaria diagnosis [150]. Others have explored novel applications like observation of neuronal network activity [151], observation and characterization of protein and colloidal aggregates [152–156], investigation of *Streptococcus mutans* biofilm microrheology [157], investigation of cell adhesion gaps in various cancer cells [158], and sensing bone cell morphogenesis under shear stress [159]. Each of these applications presents a potential area of investigation for LHM system development, and would expand the range of applications for LHM.

LHM presents a compelling technique for many clinical and biomedical applications. Its unique characteristics enable it to simultaneously replace conventional microscopic imaging techniques in many ways while also enabling novel imaging and treatment workflows. Future research in LHM would be best directed towards improving its transformative aspects, such as on-chip functionality, in-incubator approaches, 3D reconstructions, novel deep learning approaches, and translational studies to drive LHM adoption in the clinic and biomedical research.

Acknowledgements
This work was supported in part by the National Science Foundation, grant no. ECCS-2114275.

References

[1] C. Wongsrichanalai, M. J. Barcus, S. Muth, A. Sutamihardja, W. H. Wernsdorfer, *The American Journal of Tropical Medicine and Hygiene* **2007**, *77*, 6_Suppl 119.

[2] R. Huisjes, W. W. Van Solinge, M. D. Levin, R. Van Wijk, J. A. Riedl, *International Journal of Laboratory Hematology* **2018**, *40*, 2 159.

[3] S. Kamiloglu, G. Sari, T. Ozdal, E. Capanoglu, *Food Frontiers* **2020**, *1*, 3 332.

[4] S. Guida, S. Longhitano, M. Ardigò, R. Pampena, S. Ciardo, L. Bigi, V. D. Mandel, C. Vaschieri, M. Manfredini, C. Pezzini, F. Arginelli, F. Farnetani, N. Zerbinati, C. Longo, G. Pellacani, *Australasian Journal of Dermatology* **2022**, *63*, 1 15.

[5] G. Cox, *Optical Imaging Techniques in Cell Biology*, CRC Press, 2nd edition, **2012**.

[6] E. McLeod, A. Ozcan, *Reports on Progress in Physics* **2016**, *79*, 7 076001.

[7] M. K. Kim, *Journal of Photonics for Energy* **2010**, 018005.

[8] M. A. Neifeld, *Optics letters* **1998**, *23 18* 1477.

[9] M. Roy, D. Seo, S. Oh, J.-W. Yang, S. Seo, *Biosensors and Bioelectronics* **2017**, *88* 130.

[10] Y. Wu, A. Ozcan, *Methods* **2018**, *136* 4.

[11] P. Gao, C. Yuan, *Light: Advanced Manufacturing* **2022**, *3*, 1 105.

[12] D. Chen, L. Wang, X. Luo, H. Xie, X. Chen, *Photonics* **2022**, *9*, 5 358.

[13] T. Zeng, Y. Zhu, E. Y. Lam, *Optics Express* **2021**, *29*, 24 40572.

[14] W. Zhang, L. Cao, D. J. Brady, H. Zhang, J. Cang, H. Zhang, G. Jin, *Physical Review Letters* **2018**, *121*, 9 093902.

[15] D. Gabor, *Nature* **1948**, *161*, 4098 777.

[16] A. Adinda-Ougba, N. Koukourakis, N. C. Gerhardt, M. R. Hofmann, *Current Directions in Biomedical Engineering* **2015**, *1*, 1 261.

[17] O. Mudanyali, D. Tseng, C. Oh, S. O. Isikman, I. Sencan, W. Bishara, C. Oztoprak, S. Seo, B. Khademhosseini, A. Ozcan, *Lab on a Chip* **2010**, *10*, 11 1417.

[18] Z. Xiong, J. E. Melzer, J. Garan, E. McLeod, *Optics Express* **2018**, *26*, 20 25676.

[19] Z. Xiong, C. J. Potter, E. McLeod, *ACS Sensors* **2021**, *6*, 3 1208.

[20] Q. Wei, E. McLeod, H. Qi, Z. Wan, R. Sun, A. Ozcan, *Scientific Reports* **2013**, *3*, 1 1699.

[21] T.-W. Su, L. Xue, A. Ozcan, *Proceedings of the National Academy of Sciences* **2012**, *109*, 40 16018.

[22] S. Seo, S. O. Isikman, I. Sencan, O. Mudanyali, T.-W. Su, W. Bishara, A. Erlinger, A. Ozcan, *Analytical Chemistry* **2010**, *82*, 11 4621.

[23] J. W. Goodman, *Introduction to Fourier Optics*, The McGraw-Hill Companies, 2nd edition, **2005**.

[24] S. O. Isikman, I. Sencan, O. Mudanyali, W. Bishara, C. Oztoprak, A. Ozcan, *Lab on a Chip* **2010**, *10*, 9 1109.

[25] D. Coyle, L. Hampton, *Telecommunications Policy* **2024**, *48*, 1 102649.

[26] W. Bishara, T.-W. Su, A. F. Coskun, A. Ozcan, *Optics Express* **2010**, *18*, 11 11181.

[27] C. Fournier, F. Jolivet, L. Denis, N. Verrier, E. Thiebaut, C. Allier, T. Fournel, *Applied Optics* **2017**, *56*, 1 69.

[28] W. Luo, A. Greenbaum, Y. Zhang, A. Ozcan, *Light: Science & Applications* **2015**, *4*, 3 e261.

[29] M. Baker, W. Liu, E. McLeod, *Optics Express* **2021**, *29*, 14 22761.

[30] H. Lee, J. Kim, J. Kim, P. Jeon, S. A. Lee, D. Kim, *Optics Express* **2021**, *29*, 19 29996.

[31] Y. Gao, F. Yang, L. Cao, *Cells* **2022**, *11*, 13 1999.

[32] E. Sánchez-Ortiga, A. Doblas, G. Saavedra, M. Martínez-Corral, J. Garcia-Sucerquia, *Applied Optics* **2014**, *53*, 10 2058.

[33] Z. Huang, P. Memmolo, P. Ferraro, L. Cao, *PhotoniX* **2022**, *3*, 1 3.

[34] X. Wu, J. Sun, J. Zhang, L. Lu, R. Chen, Q. Chen, C. Zuo, *Optics Letters* **2021**, *46*, 9 2023.

[35] M. Rogalski, P. Arcab, L. Stanaszek, V. Mic'o, C. Zuo, M. Trusiak, *Optics express* **2023**, *32 1* 742.

[36] J. Ortiz-Ocampo, C. Trujillo, *Imaging and Applied Optics Congress 2022 (3D, AOA, COSI, ISA, pcAOP)* **2022**.

[37] Y. Zhou, X. Hua, Z. Zhang, X. Hu, K. Dixit, J. Zhong, G. Zheng, X. Cao, *Optics and Lasers in Engineering* **2020**, *134* 106131.

[38] J. K. Adams, D. Yan, J. Wu, V. Boominathan, S. Gao, A. V. Rodriguez, S. Kim, J. Carns, R. Richards-Kortum, C. Kemere, A. Veeraraghavan, J. T. Robinson, *Nature Biomedical Engineering* **2022**, *6*, 5 617.

[39] L. Chen, X. Chen, H. Cui, Y. Long, J. Wu, *Optics Communications* **2021**, *484* 126682.

[40] O. Mudanyali, C. Oztoprak, D. Tseng, A. Erlinger, A. Ozcan, *Lab on a Chip* **2010**, *10*, 18 2419.

[41] M. Rostykus, F. Soulez, M. Unser, C. Moser, *Methods* **2018**, *136* 17.

[42] M. Rogalski, J. Á. Picazo-Bueno, J. Winnik, P. Zdańkowski, V. Micó, M. Trusiak, *Scientific Reports* **2022**, *12*.

[43] F. Nette, A. C. G. de Souza, T. Laskay, M. Ohms, D. Dömer, D. Drömann, D. H. Rapoport, *PLoS ONE* **2022**, *17*.

[44] C. Tai, A. Ahmadzadegan, A. M. Ardekani, V. Narsimhan, *Soft matter* **2022**.

[45] Y. Zhang, Y. Shin, K. Sung, S. Yang, H. Chen, H. Wang, D. Teng, Y. Rivenson, R. P. Kulkarni, A. Ozcan, *Science Advances* **2017**, *3*, 8 e1700553.

[46] W. Zheng, J. Wang, Y. Zhou, Q. Zeng, C. Zhang, L. Liu, H. Yu, Y. Yang, *Optics Letters* **2023**, *48*, 3 771.

[47] F. Momey, A. Berdeu, T. Bordy, J.-M. Dinten, F. K. Marcel, N. Picollet-D'hahan, X. Gidrol, C. Allier, *Biomedical Optics Express* **2016**, *7*, 3 949.

[48] O. Ronneberger, P. Fischer, T. Brox, U-Net: Convolutional Networks for Biomedical Image Segmentation, **2015**, ArXiv:1505.04597 [cs].

[49] N. Navab, J. Hornegger, W. M. Wells, A. F. Frangi, editors, *Medical Image Computing and Computer-Assisted Intervention – MICCAI 2015: 18th International Conference, Munich, Germany, October 5-9, 2015, Proceedings, Part III*, volume 9351 of *Lecture Notes in Computer Science*, Springer International Publishing, Cham, **2015**.

[50] T. Pitkäaho, A. Manninen, T. J. Naughton, *Applied Optics* **2019**, *58*, 5 A202.

[51] Y. Wu, Y. Rivenson, Y. Zhang, Z. Wei, H. Günaydin, X. Lin, A. Ozcan, *Optica* **2018**, *5*, 6 704.

[52] L. Huang, T. Liu, X. Yang, Y. Luo, Y. Rivenson, A. Ozcan, *ACS Photonics* **2021**, *8*, 6 1763.

[53] Y. Wu, A. Ray, Q. Wei, A. Feizi, X. Tong, E. Chen, Y. Luo, A. Ozcan, *ACS Photonics* **2019**, *6*, 2 294.

[54] M. Montoya, M. J. Lopera, A. Gómez-Ramírez, C. Buitrago-Duque, A. Pabón-Vidal, J. Herrera-Ramirez, J. Garcia-Sucerquia, C. Trujillo, *Optics and Lasers in Engineering* **2023**, *165* 107546.

[55] J. Chen, W. Han, L. Fu, Z. Lv, H. Chen, W. Fang, J. Hou, H. Yu, X. Huang, L. Sun, *IEEE Photonics Journal* **2024**, 1–8.

[56] Y. Wu, L. Lu, J. Zhang, Z. Li, C. Zuo, *Frontiers in Physics* **2021**, *9* 651316.

[57] C. J. Potter, Y. Hu, Z. Xiong, J. Wang, E. McLeod, *Lab on a Chip* **2022**, *22*, 19 3744.

[58] R. Vaghashiya, S. Shin, V. Chauhan, K. Kapadiya, S. Sanghavi, S. Seo, M. Roy, *Biosensors* **2022**, *12*, 3 144.

[59] Z. Luo, A. Yurt, R. Stahl, A. Lambrechts, V. Reumers, D. Braeken, L. Lagae, *Optics Express* **2019**, *27*, 10 13581.

[60] Y. Rivenson, T. Liu, Z. Wei, Y. Zhang, K. De Haan, A. Ozcan, *Light: Science & Applications* **2019**, *8*, 1 23.

[61] M. A. Pala, M. E. Çimen, A. Akgül, M. Z. Yıldız, A. F. Boz, *The European Physical Journal Special Topics* **2022**, *231*, 5 1023.

[62] Y. Luo, H.-A. Joung, S. Esparza, J. Rao, O. Garner, A. Ozcan, *Lab on a Chip* **2021**, *21*, 18 3550.

[63] C. Allier, L. Hervé, C. Paviolo, O. Mandula, O. Cioni, W. Pierré, F. Andriani, K. Padmanabhan, S. Morales, *Frontiers in Physics* **2022**, *9* 776805.

[64] H. Zhu, O. Yaglidere, T.-W. Su, D. Tseng, A. Ozcan, *Lab Chip* **2011**, *11*, 2 315.

[65] J. C. Contreras-Naranjo, Q. Wei, A. Ozcan, *IEEE Journal of Selected Topics in Quantum Electronics* **2016**, *22*, 3 1.

[66] A. Greenbaum, Y. Zhang, A. Feizi, P.-L. Chung, W. Luo, S. R. Kandukuri, A. Ozcan, *Science Translational Medicine* **2014**, *6*, 267.

[67] Y. Zhang, T. Liu, Y. Huang, D. Teng, Y. Bian, Y. Wu, Y. Rivenson, A. Feizi, A. Ozcan, *Journal of Biophotonics* **2019**, *12*, 3 e201800335.

[68] G. Zeng, J. He, W. Qin, *Frontiers in Oncology* **2021**, *11* 751223.

[69] T. Liu, Z. Wei, Y. Rivenson, K. De Haan, Y. Zhang, Y. Wu, A. Ozcan, *Journal of Biophotonics* **2019**, *12*, 11 e201900107.

[70] H. Shen, J. Gao, *Chinese Optics Letters* **2020**, *18*, 12 121705.

[71] C. Guo, X. Liu, X. Kan, F. Zhang, J. Tan, S. Liu, Z. Liu, *Optics Express* **2019**, *27*, 24 35216.

[72] C. Guo, X. Liu, X. Kan, F. Zhang, J. Tan, S. Liu, C. Tan, Z. Liu, *Measurement Science and Technology* **2020**, *31*, 4 045402.

[73] C. Guo, F. Zhang, X. Zhang, X. Kan, J. Tan, S. Liu, Z. Liu, *Journal of Optics* **2020**, *22*, 5 055703.

[74] Y. Zhang, H. Wang, Y. Wu, M. Tamamitsu, A. Ozcan, *Optics Letters* **2017**, *42*, 19 3824.

[75] Y. Rivenson, Y. Zhang, H. Günaydın, D. Teng, A. Ozcan, *Light: Science & Applications* **2018**, *7*, 2 17141.

[76] H. Chen, L. Huang, T. Liu, A. Ozcan, *Light: Science & Applications* **2022**, *11*, 1 254.

[77] T. Liu, K. De Haan, Y. Rivenson, Z. Wei, X. Zeng, Y. Zhang, A. Ozcan, *Scientific Reports* **2019**, *9*, 1 3926.

[78] J. A. Picazo-Bueno, K. Trindade, M. Sanz, V. Micó, *Sensors* **2022**, *22*, 2 553.

[79] M. J. Lopera, C. Trujillo, *Applied Optics* **2022**, *61*, 5 B77.

[80] Y. Zhang, S. Y. C. Lee, Y. Zhang, D. Furst, J. Fitzgerald, A. Ozcan, *Scientific Reports* **2016**, *6*, 1 28793.

[81] T. Liu, K. de Haan, B. Bai, Y. Rivenson, Y. Luo, H. Wang, D. Karalli, H. Fu, Y. Zhang, J. FitzGerald, A. Ozcan, *ACS Photonics* **2020**, *7*, 11 3023.

[82] J. Kun, M. Smieja, B. Xiong, L. Soleymani, Q. Fang, *Scientific Reports* **2019**, *9*, 1 17255.

[83] C. Pacheco, G. N. McKay, A. Oommen, N. J. Durr, R. Vidal, B. D. Haeffele, *Optics Express* **2022**, *30*, 19 33433.

[84] G. N. McKay, A. Oommen, C. Pacheco, M. T. Chen, S. C. Ray, R. Vidal, B. D. Haeffele, N. J. Durr, *IEEE Transactions on Biomedical Engineering* **2023**, *70*, 3 1053.

[85] R. Delacroix, S. N. A. Morel, L. Hervé, T. Bordy, J.-M. Dinten, M. Drancourt, C. Allier, *Scientific Reports* **2017**, *7*, 1 39893.

[86] M. Khaleghi, C. Furlong, M. Ravicz, J. T. Cheng, J. J. Rosowski, *Journal of Biomedical Optics* **2015**, *20*, 5 051028.

[87] M. Baker, E. McLeod, *APL Photonics* **2023**, *8*, 6 061301.

[88] P. Arcab, M. Rogalski, M. Trusiak, *Optics and Lasers in Engineering* **2024**, *172* 107878.

[89] Y. Li, B. Cornelis, A. Dusa, G. Vanmeerbeeck, D. Vercruysse, E. Sohn, K. Blaszkiewicz, D. Prodanov, P. Schelkens, L. Lagae, *Computers in Biology and Medicine* **2018**, *96* 147.

[90] S. Amann, M. V. Witzleben, S. Breuer, *Scientific Reports* **2019**, *9*, 1 11260.

[91] H. Tobon-Maya, S. Zapata-Valencia, E. Zora-Guzmán, C. Buitrago-Duque, J. Garcia-Sucerquia, *Applied Optics* **2021**, *60*, 4 A205.

[92] C. Buitrago-Duque, B. Patiño-Jurado, J. Garcia-Sucerquia, *HardwareX* **2023**, *13* e00408.

[93] B. Patiño-Jurado, J. F. Botero-Cadavid, J. Garcia-Sucerquia, *Applied Optics* **2020**, *59*, 10 2969.

[94] M. J. Lopera, C. Trujillo, *Optics Letters* **2022**, *47*, 11 2862.

[95] A. C. Sobieranski, F. Inci, H. C. Tekin, M. Yuksekkaya, E. Comunello, D. Cobra, A. Von Wangenheim, U. Demirci, *Light: Science & Applications* **2015**, *4*, 10 e346.

[96] W. Bishara, U. Sikora, O. Mudanyali, T.-W. Su, O. Yaglidere, S. Luckhart, A. Ozcan, *Lab on a Chip* **2011**, *11*, 7 1276.

[97] Y. Fang, N. Yu, Y. Jiang, *Applied Sciences* **2019**, *9*, 10 2080.

[98] H. P. R. Gurram, A. S. Galande, R. John, *Optical Engineering* **2020**, *59*, 10.

[99] Y. Huang, M. Zhu, L. Ma, W. Zhang, *Optics Communications* **2023**, *526* 128898.

[100] M. Sanz, J. A. Picazo-Bueno, J. García, V. Micó, *Optics Express* **2015**, *23*, 16 21352.

[101] M. Sanz, J. Picazo-Bueno, L. Granero, J. García, V. Micó, *Scientific Reports* **2017**, *7*, 1 43291.

[102] M. Sanz, J. A. Picazo-Bueno, J. García, V. Micó, *Lab on a Chip* **2018**, *18*, 7 1105.

[103] Y. Fang, N. Yu, Y. Jiang, C. Dang, *Micromachines* **2018**, *9*, 5 227.

[104] B. Cornelis, D. Blinder, B. Jansen, L. Lagae, P. Schelkens, *Optics Express* **2018**, *26*, 11 14329.

[105] D. Ahn, J. Lee, S. Moon, T. Park, *The Analyst* **2018**, *143*, 22 5380.

[106] X. Huang, Y. Li, X. Xu, R. Wang, J. Yao, W. Han, M. Wei, J. Chen, W. Xuan, L. Sun, *Sensors* **2021**, *21*, 3 720.

[107] T. O'Connor, C. Hawxhurst, L. M. Shor, B. Javidi, *Optics Express* **2020**, *28*, 22 33504.

[108] Y. Zhang, M. Ouyang, A. Ray, T. Liu, J. Kong, B. Bai, D. Kim, A. Guziak, Y. Luo, A. Feizi, K. Tsai, Z. Duan, X. Liu, D. Kim, C. Cheung, S. Yalcin, H. Ceylan Koydemir, O. B. Garner, D. Di Carlo, A. Ozcan, *Light: Science & Applications* **2019**, *8*, 1 91.

[109] D. Vercruysse, A. Dusa, R. Stahl, G. Vanmeerbeeck, K. De Wijs, C. Liu, D. Prodanov, P. Peumans, L. Lagae, *Lab on a Chip* **2015**, *15*, 4 1123.

[110] D. Seo, S. Oh, M. Lee, Y. Hwang, S. Seo, *Sensors* **2017**, *18*, 2 85.

[111] G. Huang, Z. Liu, G. Pleiss, L. V. D. Maaten, K. Q. Weinberger, *IEEE Transactions on Pattern Analysis and Machine Intelligence* **2019**, *44*, 12 8704.

[112] T. Liu, Y. Li, H. C. Koydemir, Y. Zhang, E. Yang, M. Eryilmaz, H. Wang, J. Li, B. Bai, G. Ma, A. Ozcan, *Nature Biomedical Engineering* **2023**, *7*, 8 1040.

[113] S. Seo, T.-W. Su, D. K. Tseng, A. Erlinger, A. Ozcan, *Lab Chip* **2009**, *9*, 6 777.

[114] T. E. Agbana, H. Gong, A. S. Amoah, V. Bezzubik, M. Verhaegen, G. Vdovin, *Optics Letters* **2017**, *42*, 12 2271.

[115] Y. Zhang, H. Ceylan Koydemir, M. M. Shimogawa, S. Yalcin, A. Guziak, T. Liu, I. Oguz, Y. Huang, B. Bai, Y. Luo, Y. Luo, Z. Wei, H. Wang, V. Bianco, B. Zhang, R. Nadkarni, K. Hill, A. Ozcan, *Light: Science & Applications* **2018**, *7*, 1 108.

[116] C. D. P. DAlmeida, K. J. Sammarro Silva, L. P. Sabogal-Paz, S. Pratavieira, *Journal of Environmental Chemical Engineering* **2023**, *11*, 5 110932.

[117] E. Serabyn, K. Liewer, C. Lindensmith, K. Wallace, J. Nadeau, *Optics Express* **2016**, *24*, 25 28540.

[118] S. Ebrahimi, M. Dashtdar, *Optics Letters* **2021**, *46*, 15 3516.

[119] M. Rostykus, C. Moser, *Optics Express* **2017**, *25*, 14 16652.

[120] A. Ray, M. U. Daloglu, J. Ho, A. Torres, E. Mcleod, A. Ozcan, *Scientific Reports* **2017**, *7*, 1 4856.

[121] O. Mudanyali, E. McLeod, W. Luo, A. Greenbaum, A. F. Coskun, Y. Hennequin, C. P. Allier, A. Ozcan, *Nature Photonics* **2013**, *7*, 3 247.

[122] A. Ray, M. A. Khalid, A. Demčenko, M. Daloglu, D. Tseng, J. Reboud, J. M. Cooper, A. Ozcan, *Nature Communications* **2020**, *11*, 1 171.

[123] H. Wang, H. Ceylan Koydemir, Y. Qiu, B. Bai, Y. Zhang, Y. Jin, S. Tok, E. C. Yilmaz, E. Gumustekin, Y. Rivenson, A. Ozcan, *Light: Science & Applications* **2020**, *9*, 1 118.

[124] P. Perlemoine, P. R. Marcoux, E. Picard, E. Hadji, M. Zelsmann, G. Mugnier, A. Marchet, G. Resch, L. O'Connell, E. Lacot, *PLOS ONE* **2021**, *16*, 3 e0248917.

[125] M. Veli, A. Ozcan, *ACS Nano* **2018**, *12*, 3 2554.

[126] F. Colle, D. Vercruysse, S. Peeters, C. Liu, T. Stakenborg, L. Lagae, J. Del-Favero, *Lab on a Chip* **2013**, *13*, 21 4257.

[127] A. Berdeu, B. Laperrousaz, T. Bordy, O. Mandula, S. Morales, X. Gidrol, N. Picollet-D'hahan, C. Allier, *Scientific Reports* **2018**, *8*, 1 16135.

[128] A. Berdeu, F. Momey, B. Laperrousaz, T. Bordy, X. Gidrol, J.-M. Dinten, N. Picollet-D'hahan, C. Allier, *Applied Optics* **2017**, *56*, 13 3939.

[129] G. Scholz, S. Mariana, A. Dharmawan, I. Syamsu, P. Hörmann, C. Reuse, J. Hartmann, K. Hiller, J. Prades, H. Wasisto, A. Waag, *Sensors* **2019**, *19*, 5 1234.

[130] L. Ghenim, C. Allier, P. Obeid, L. Hervé, J.-Y. Fortin, M. Balakirev, X. Gidrol, *Scientific Reports* **2021**, *11*, 1 1290.

[131] S. V. Kesavan, F. P. Navarro Y Garcia, M. Menneteau, F. Mittler, B. David-Watine, N. Dubrulle, S. L. Shorte, B. Chalmond, J.-M. Dinten, C. P. Allier, *Journal of Biomedical Optics* **2014**, *19*, 03 1.

[132] A. B. Dharmawan, S. Mariana, G. Scholz, P. Hörmann, T. Schulze, K. Triyana, M. Garcés-Schröder, I. Rustenbeck, K. Hiller, H. S. Wasisto, A. Waag, *Scientific Reports* **2021**, *11*, 1 3213.

[133] I. Pushkarsky, Y. Liu, W. Weaver, T.-W. Su, O. Mudanyali, A. Ozcan, D. Di Carlo, *Scientific Reports* **2014**, *4*, 1 4717.

[134] C. Allier, S. Morel, R. Vincent, L. Ghenim, F. Navarro, M. Menneteau, T. Bordy, L. Hervé, O. Cioni, X. Gidrol, Y. Usson, J.-M. Dinten, *Cytometry Part A* **2017**, *91*, 5 433.

[135] C. Allier, R. Vincent, F. Navarro, M. Menneteau, L. Ghenim, X. Gidrol, T. Bordy, L. Hervé, O. Cioni, S. Bardin, M. Bornens, Y. Usson, S. Morales, *Journal of Visualized Experiments* **2018**, , 132 56580.

[136] B. Mirecki, M. Rogalski, P. Arcab, P. Rogujski, L. Stanaszek, M. Józwik, M. Trusiak, *Biomedical Optics Express* **2022**, *13*, 11 5667.

[137] G. Li, R. Zhang, N. Yang, C. Yin, M. Wei, Y. Zhang, J. Sun, *Biosensors and Bioelectronics* **2018**, *107* 163.

[138] M. A. Kabir, A. Kharel, S. Malla, Z. J. Kreis, P. Nath, J. N. Wolfe, M. Hassan, D. Kaur, H. Sari-Sarraf, A. K. Tiwari, A. Ray, *Journal of Biophotonics* **2022**, *15*, 4.

[139] M. Falck Miniotis, A. Mukwaya, A. Gjörloff Wingren, *PLoS ONE* **2014**, *9*, 9 e106546.

[140] R. Boltyanskiy, M. A. Odete, F. C. Cheong, L. A. Philips, *Scientific Reports* **2022**, *12*, 1 12746.

[141] K. Delikoyun, S. Yaman, E. Yilmaz, O. Sarigil, M. Anil-Inevi, K. Telli, O. Yalcin-Ozuysal, E. Ozcivici, H. C. Tekin, *ACS Sensors* **2021**, *6*, 6 2191.

[142] M. Wang, S. Feng, J. Wu, *Scientific Reports* **2017**, *7*, 1 12791.

[143] S. O. Isikman, A. Greenbaum, W. Luo, A. F. Coskun, A. Ozcan, *PLoS ONE* **2012**, *7*, 9 e45044.

[144] S. I. Zapata-Valencia, H. Tobon-Maya, J. Garcia-Sucerquia, *Journal of the Optical Society of America A* **2023**, *40*, 4 C150.

[145] H. Tobon, C. Trujillo, J. Garcia-Sucerquia, *Applied Optics* **2021**, *60*, 4 A215.

[146] C. A. Trujillo, J. Garcia-Sucerquia, *Optics Letters* **2014**, *39*, 9 2569.

[147] D. Ryu, Z. Wang, K. He, G. Zheng, R. Horstmeyer, O. Cossairt, *Biomedical Optics Express* **2017**, *8*, 3 1981.

[148] M. Ugele, M. Weniger, M. Stanzel, M. Bassler, S. W. Krause, O. Friedrich, O. Hayden, L. Richter, *Advanced Science* **2018**, *5*, 12 1800761.

[149] P. Memmolo, G. Aprea, V. Bianco, R. Russo, I. Andolfo, M. Mugnano, F. Merola, L. Miccio, A. Iolascon, P. Ferraro, *Biosensors and Bioelectronics* **2022**, *201* 113945.

[150] M. Ugele, M. Weniger, M. Leidenberger, Y. Huang, M. Bassler, O. Friedrich, B. Kappes, O. Hayden, L. Richter, *Lab on a Chip* **2018**, *18*, 12 1704.

[151] P. Marquet, C. Depeursinge, P. J. Magistretti, *Neurophotonics* **2014**, *1*, 2 020901.

[152] C. Wang, X. Zhong, D. B. Ruffner, A. Stutt, L. A. Philips, M. D. Ward, D. G. Grier, *Journal of Pharmaceutical Sciences* **2016**, *105*, 3 1074.

[153] C. Wang, F. C. Cheong, D. B. Ruffner, X. Zhong, M. D. Ward, D. G. Grier, *Soft Matter* **2016**, *12*, 42 8774.

[154] A. Wang, J. W. Zwanikken, D. M. Kaz, R. McGorty, A. M. Goldfain, W. B. Rogers, V. N. Manoharan, *Physical Review E* **2019**, *100*, 4 042605.

[155] L. E. Altman, D. G. Grier, *The Journal of Physical Chemistry B* **2020**, acs.jpcb.9b10463.

[156] M. D. Hannel, A. Abdulali, M. O'Brien, D. G. Grier, *Optics Express* **2018**, *26*, 12 15221.

[157] F. C. Cheong, S. Duarte, S.-H. Lee, D. G. Grier, *Rheologica Acta* **2009**, *48*, 1 109.

[158] S. Dai, T. Yu, J. Zhang, H. Lu, J. Dou, M. Zhang, C. Dong, J. Di, J. Zhao, *Biosensors and Bioelectronics* **2021**, *174* 112826.

[159] W. Xiao, L. Xin, R. Cao, X. Wu, R. Tian, L. Che, L. Sun, P. Ferraro, F. Pan, *Lab on a Chip* **2021**, *21*, 7 1385.

Colin J. Potter received a B.S. in neuroscience and cognitive science and in molecular and cellular biology in 2018 and a M.S. in optical sciences in 2022, both from the University of Arizona, Tucson.
He worked as a Research Assistant in the Koshy Lab studying the parasitic interaction of *Toxoplasma gondii* with the nervous system from 2015 through 2018. In 2017, he worked as a Research Assistant at Neuroscience Research Australia in Sydney, Australia. He is currently a student in the University of Arizona College of Medicine - Tucson Medical Scientist Training Program, or M.D./Ph.D. Program, which he started in 2018 and is expected to graduate from in 2026.
His current research interests involve the development of optical biomedical technologies for clinical applications, which is informed by his past experience in biomedical research and his clinical training.
Mr. Potter was the recipient of an National Institutes of Health T32 training award and is an Achievement Rewards for College Scientists (ARCS) Foundation Scholar.

Zhen Xiong received a B.E. in electronic and communication engineering in 2014 from City University of Hong Kong. Afterwards he received a M.S. and a Ph.D. in optical sciences in 2017 and 2020 respectively, both from the University of Arizona.
From 2014 to 2020, he was a Research Assistant with the Soft Nano-photonic Systems Laboratory. He worked at Apple Inc. from 2020 to 2022 as an Display Optical Engineer. He currently works at Applied Materials Inc. as a Physicist/Scientist in Santa Clara. His research interests include holographic microscopy, computational imaging, and display technologies.

Euan McLeod received a Bachelor's of Science in mechanical engineering from the California Institute of Technology in Pasadena, CA, USA in 2004; and a Ph.D. in mechanical and aerospace engineering from Princeton University in Princeton, NJ, USA in 2009.
Since 2021, he has been an Associate Professor of Optical Sciences at the University of Arizona. He is also an Associate Professor of the UA BIO5 Institute and an Affiliate Member of the UA Cancer Center. Prior to becoming an associate professor, he joined the University of Arizona as an Assistant Professor of Optical Sciences in 2015. From 2011–2014, he was a Postdoctoral Scholar at the University of California, Los Angeles in the Electrical Engineering department. From 2009-2011, he was a Postdoctoral Scholar in Applied Physics at the California Institute of Technology. His background and interests lie at the intersection of optics, nanoscience, and soft bio-materials science. He has published more than 40 papers on these topics in peer-reviewed journals and has been awarded 6 patents, with major contributions in the areas of high-speed varifocal lenses based on acoustic modulation, lensfree holographic imaging of nanoparticles, viruses, and biomarkers; and the use of optical tweezers in fabricating micro- and nano-structured materials.
Prof. McLeod is a Senior Member of both SPIE and Optica. He won an NSF CAREER award in 2021.

Table of Contents

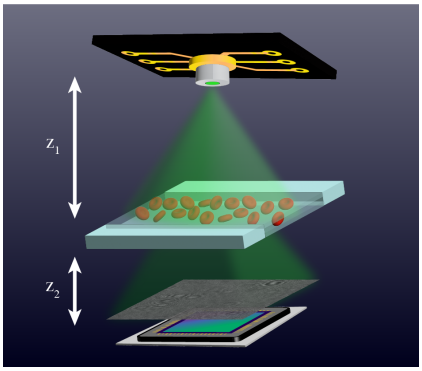

Lensless holographic microscopy is a powerful imaging technique that has been used in a wide range of applications relevant to clinical medicine and biomedical research. This review provides a comprehensive summary of recent successful applications of this technique and their significance to biomedicine.